

---

# A pure sliding experiment to examine wear on possible coatings for greaseless open gears

---

NIEK REULING  
MASTER THESIS  
NOVEMBER 2024

UNIVERSITY OF TWENTE.



**Supervisors:**

DR. A. VRČEK  
DR. N.F. BADER  
PROF. DR. IR. M.B. DE ROOIJ

MECHANICAL ENGINEERING  
FACULTY OF ENGINEERING TECHNOLOGY  
SURFACE TECHNOLOGY AND TRIBOLOGY



## Acknowledgements

I would like to thank Aleks Vrčec, my supervisor at Huisman and Norbert Bader, my supervisor at the University of Twente for the support and insights in during this project. Both were always able to find time to answer questions and that helped a lot.

Also, I would like to thank Erik de Vries and Robert Jan Meijer for their help during the experimental setup phase and for providing useful practical tips and codes.

Lastly, I would like to thank Matthijn de Rooij for his useful feedback and guidance during this thesis.



## Summary

In the offshore industry, ships have gear systems to ensure the rotation and translation required during operation. Current systems use grease to reduce friction and wear. Grease can spill into the sea out of these systems, harming nature even with biodegradable greases as these are not 100% biodegradable. This mainly happens in open systems, such as rack-pinion systems. The lubrication type present theoretically is boundary lubrication. A solution to this problem should still include a friction- and wear-reducing layer. A greaseless open gear system would solve grease-spilling problems. A proposed solution is to coat the pinion with a laser-clad added cobalt-based superalloy. The coatings are stellite 21, stellite 6 and stellite 190. These typically show a low wear rate and friction coefficient, which is required as it should replace grease properties. Besides, a high bond strength can be reached.

In this study, tribological experiments are performed to study the effect of various parameters on the type and severity of wear of the proposed coatings and base case with the corresponding coefficient of friction. This gives insight into the performance of the coatings relative to each other and to the base case and how this changes with different parameters. Wear and friction are system properties so to determine the quality of the coatings, it should be experimented on, mimicking the real system. To do this, the real contact conditions are matched based on an analysis of the real system. Different types of wear can be present in a system: abrasive, adhesive, corrosive, and rolling contact fatigue.

A combination of rolling and sliding is present in a real gear system, leading to a slide-to-roll ratio (SRR). In these experiments, however, pure sliding is experimented. A disc-on-disc experiment on the UMT Tribolab is used for this. One disc is stationary and creates a wear track on a rotating disc. The (coated) pinion material is the stationary disc and the rack material is the rotating disc. The influence of different parameters is assessed. Different types of lubrication are experimented with, namely no lubrication, purified water, seawater and grease to have a base case. The influence of load and velocity is experimented with. At last, the influence of hardness is experimented with. After the wear experiments are carried out, the height profile of the wear track is measured with a profilometer. This is in Matlab analysed to calculate the specific wear rate. To determine the type of wear, the morphology of the wear track surface is also observed and together with the wear rate, this can tell the type of wear. Friction is analysed to further increase understanding of the phenomena happening, and this value must be low as the coatings replace the grease.

The proposed laser clad cobalt-based superalloy coatings do reduce wear compared to the uncoated material. Stellite 190 is found to be the best wear-reducing. Unlubricated wear is undesirable as severe adhesive wear is present. (Sea)water lubrication shows better performance. However, the uncoated pinion with grease lubrication which is the current situation in the observed applications performs better in terms of wear and friction because boundary lubrication is present. It is found that a higher velocity leads to less wear. The reason could be corrosive wear and build-up of an oxide layer. A higher load leads to more plastic deformation, however, the specific wear rate will be a lower value due to normalisation over the load. A hardness increase in the coatings decreases the wear only with similar material composition. The base material in the same conditions shows more wear but has a higher hardness.

It is still to be determined if the wear reduction by the coatings is enough to be feasible as a replacement for grease in offshore applications.



---

## Contents

<b>Acknowledgements</b>	<b>I</b>
<b>Summary</b>	<b>II</b>
<b>1 Introduction</b>	<b>1</b>
1.1 Problem statement . . . . .	1
1.2 Aim and objective . . . . .	2
1.3 Scope of the research . . . . .	2
1.4 Applications . . . . .	2
1.4.1 Motion- compensated Pile Gripper . . . . .	2
1.4.2 Slew Bearing . . . . .	3
1.4.3 Winch drive . . . . .	4
<b>2 Literature review</b>	<b>5</b>
2.1 Tribological system . . . . .	5
2.2 Contact . . . . .	5
2.3 Lubrication . . . . .	7
2.4 Friction . . . . .	9
2.5 Wear . . . . .	12
2.6 Gear kinematics and tribology . . . . .	16
2.7 Possible solutions . . . . .	19
2.7.1 Laser cladding . . . . .	20
2.7.2 Possible laser-cladded coatings . . . . .	21
<b>3 Research questions</b>	<b>22</b>
<b>4 Current system properties</b>	<b>23</b>
4.1 Roughness . . . . .	23
4.2 Grease . . . . .	23
4.3 Contact pressure . . . . .	24
4.4 Sliding velocity . . . . .	24
4.5 Lubrication regime . . . . .	24
4.6 Sliding distance . . . . .	25
4.7 Environment . . . . .	26
<b>5 Experimental materials and methodology</b>	<b>27</b>
5.1 Measurement inputs and materials . . . . .	27
5.1.1 Lubrication . . . . .	28
5.1.2 Materials . . . . .	29
5.1.3 Cleaning . . . . .	29
5.1.4 Hardness measurements . . . . .	29
5.1.5 Grouping of velocities and loads into experimental cases . . . . .	30
5.1.5.1 Calculating loads . . . . .	30
5.1.6 Sliding distance . . . . .	31
5.1.7 Experimental matrix . . . . .	32
5.2 Data measurement . . . . .	33
5.3 Data processing . . . . .	33
5.3.1 Rotating disc . . . . .	33

---

5.3.2	Stationary disc . . . . .	34
5.3.3	Roughness . . . . .	37
5.3.4	Coefficient of friction . . . . .	37
<b>6</b>	<b>Experimental results</b>	<b>39</b>
6.1	Hardness measurements . . . . .	39
6.2	Roughness . . . . .	39
6.3	Wear and Coefficient of Friction results . . . . .	39
6.3.1	The influence of different types of lubrication . . . . .	39
6.3.2	The influence of load . . . . .	45
6.3.3	The influence of velocity . . . . .	48
6.3.4	The influence of the hardness of the rack and pinion material . . . . .	51
<b>7</b>	<b>Discussion</b>	<b>57</b>
7.1	Hardness . . . . .	57
7.2	Wear analysis . . . . .	57
7.3	Onset of plasticity at the surface . . . . .	59
7.4	Invalid results . . . . .	60
7.5	Validity of the results used in this research . . . . .	61
7.5.1	Number of measured spots . . . . .	61
7.5.2	Influence of plasticity on measured wear . . . . .	61
7.5.3	Pinion material shape . . . . .	61
7.5.4	Different shape on the uncoated disc than other pinion discs . . . . .	62
7.5.5	Seawater standards . . . . .	62
7.6	Limitations of the research . . . . .	62
7.6.1	No slide-to-roll ratio . . . . .	62
7.6.2	1-directional wear . . . . .	63
7.6.3	Sliding distance . . . . .	63
7.7	Future research . . . . .	63
7.7.1	Hypotheses of formation of oxides . . . . .	63
7.7.2	Match hardness of steel and stellite . . . . .	63
7.7.3	Hardness increase of rotating disc . . . . .	63
7.7.4	Slide-to-roll ratio included in experiments . . . . .	64
7.7.5	Calculate if the wear reduction is enough . . . . .	64
7.7.6	Additives to the water . . . . .	64
<b>8</b>	<b>Conclusion</b>	<b>65</b>
<b>A</b>	<b>Cracking and chipping on production</b>	<b>71</b>

# 1 Introduction

In the offshore industry, ships have specialised equipment to install and maintain various systems such as offshore windmills. This equipment needs rotation and translation motion, which can result in problems as the marine environment is very difficult and protected because of marine life.

## 1.1 Problem statement

Grease is used to reduce friction and wear in high-loaded sliding and rotating systems. In some applications, it cannot be avoided that the grease will spill out of the system. In offshore applications, this means it will come into the sea. Current biodegradable greases are not 100 % biodegradable. A minimum biodegradability of 70 % in 28 days [1] is reached in one of the used greases, meaning the rest can still be harmful to nature. These situations are mainly present in so-called 'Open systems', where no completely closed casing is possible. At high contact pressures, the grease is moved (partially) out of the contact. However, due to the bleeding of oil from the moved grease into the contact and steel-bonding additives theoretically, a thin lubricating film is even present in these systems [2] [3]. This reduces the friction and wear. When finding a solution, a friction- and wear-reducing layer should be present, to minimise wear, stress and in the end failure.

A type of open system is a rack-and-pinion system. A pinion (gear) is rotated which causes the rack to move linearly. A schematic figure of a rack-pinion system is shown in Figure 1.1.

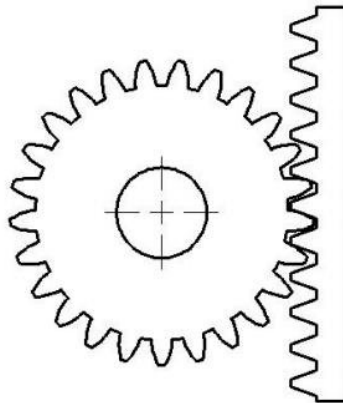


Figure 1.1: Schematic figure rack-pinion system [4]

A jacking system is one of the open systems used in the offshore industry. This jacking system uses a rack-pinion system to lower a boom to the bottom of the sea. In that way, it pushes the ship up and creates a stable plateau. The ship will not sway anymore. This stable plateau makes installing windmills easier, as they are connected to the ground and non-moving. An example of this is shown in Figure 1.5, where a ship is carried above the sea. 4 gearboxes are typically used per ship, each connected to a boom.



Figure 1.2: Jacking system demonstrated [5]

On one ship with a Jacking system, annually 7332 kg of grease is used in all the jacking systems on this ship. Most of it is spilt into the sea. For other open systems, this value is lower so the biggest impact can be made and is required for a jacking system. However, some of these systems will also be evaluated in this research and will be discussed in subsection 1.4.

A greaseless open gear system would solve the problems with grease. A proposed solution is to coat the pinion with a laser-clad added cobalt-based superalloy. This typically shows a low wear rate and friction coefficient that is required as it should replace grease properties [6][7]. These values are however, system properties and thus can be different in value per system. Therefore it is required to know exact values and characteristics applied to the researched offshore systems.

## 1.2 Aim and objective

This research aims to properly perform tribological experiments and study the effect of various parameters on the type and severity of wear of the proposed coatings and base case, and the corresponding coefficient of friction. This gives insight into the performance of the coatings relative to each other and to the base case and how this changes with different parameters.

## 1.3 Scope of the research

This research will mainly concentrate on the wear results, where friction could help to determine wear characteristics but will be studied in less detail. General corrosion will not be studied in much detail. Temperature differences will not be studied as only room temperature (20 degrees Celsius) will be used.

## 1.4 Applications

Huisman selected several interesting applications that will be used for this research. These applications will be used to determine experimental parameters. Other applications than the jacking system, which is already explained are shown below.

### 1.4.1 Motion- compensated Pile Gripper

This is a system that is used to place monopiles for windmills. It can compensate in  $x$ ,  $y$ , and  $z$  directions for waves, so no jacking system is required anymore to create a stable platform. Previously discussed rack-pinion systems perform the motions.

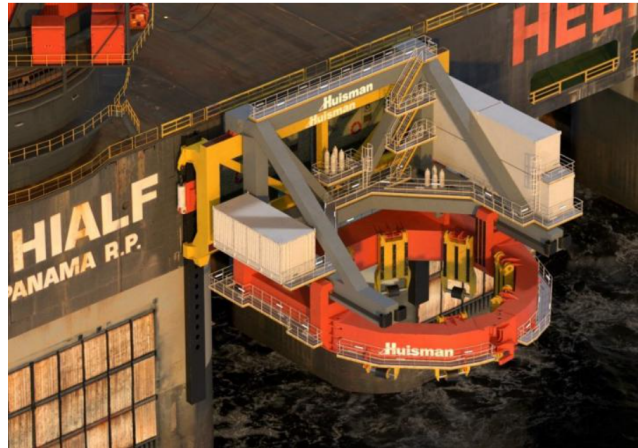


Figure 1.3: Motion- compensated pile gripper

### 1.4.2 Slew Bearing

This is the bearing that allows a crane to rotate around. It consists of a smaller gear that powers a bigger gear that has teeth on the inside. Usually, in offshore these rings are very big. In 1.4b can be seen that the pinions (connected on the white pillars, are very small compared to the slew bearing itself (the big ring).



(a) Slew bearing mounted on a crane



(b) Slew bearing assembly

Figure 1.4: Slew bearing

### 1.4.3 Winch drive

This is the system that powers the drum of the hoisting system. Wire ropes are connected that increase or decrease in length as they unwind or wind respectively, by rotating the drum. This allows a hook to be lowered or raised. It consists of small powered gears, connected to a gear with teeth on the inside like the slew bearing. However, now the drum that stores and hoists the wire rope is connected.



Figure 1.5: 2 Winches with electromotors with gears connected to the sides of the winch

## 2 Literature review

This section addresses relevant concepts, techniques and backgrounds.

### 2.1 Tribological system

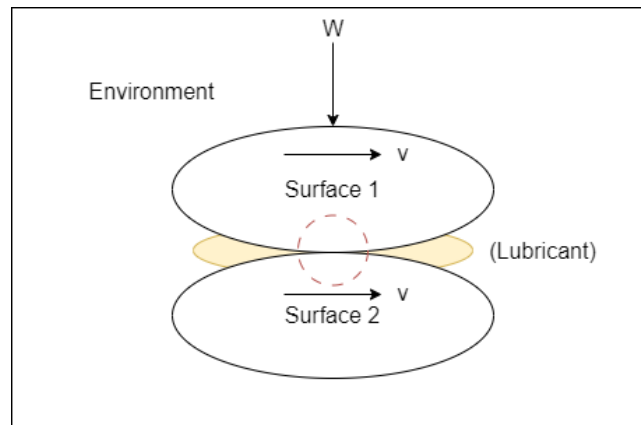


Figure 2.1: Tribological system (reproduced from [8])

Friction and wear are system properties and are connected. The system these are connected to is a tribological system which can be seen in Figure 2.1. In such a tribological system, 2 surfaces of certain materials with their properties are in contact with a possible lubricant or particles in between. Furthermore, a load and motion are acting on the surfaces. The environment consists of a certain temperature and pressure. Besides different types of environments with very specific properties (acidity, corrosive environment, etc.) can be present. Thus exactly identically tribological systems are very hard to achieve.

### 2.2 Contact

The contact pressures for rack-pinion systems can be calculated using the Herzian contact theorem for line contacts. Gears will share contact which is a line with  $2b$  width where the surfaces meet, over the complete depth  $l$  of the gear (respectively the red line in Figure 2.2 and arrow in Figure 2.3).

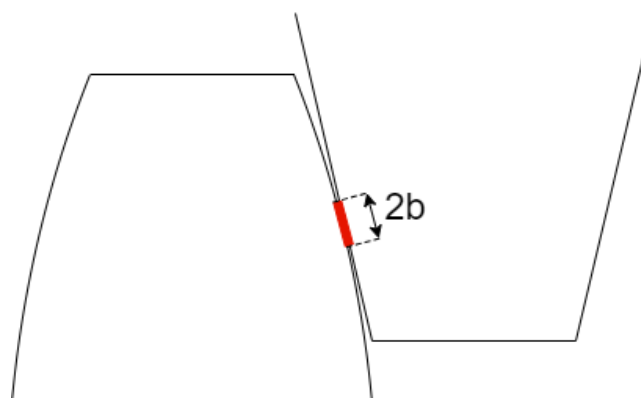


Figure 2.2: Shared contact width of gears

The pinion has a curved surface (radius of curvature) while the rack has a flat side. This can thus be modelled as a cylinder on flat contact.

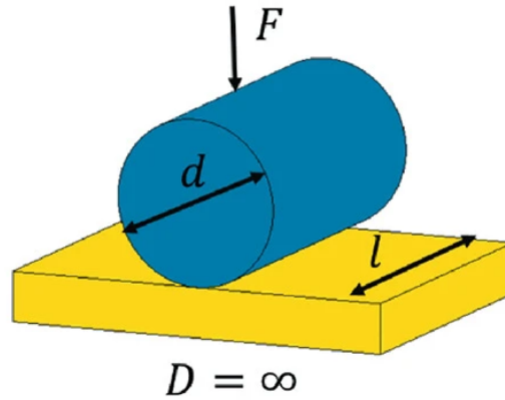


Figure 2.3: Cylinder on flat [9]

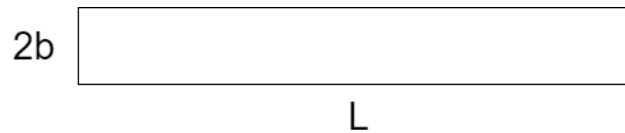


Figure 2.4: Contact area with dimensions

The half-width  $b$  of a line contact calculated with Hertz's theory is [3]:

$$b = \left( \frac{F}{L} \frac{4R'_x}{\pi E'} \right)^{\frac{1}{2}} \quad (1)$$

Where  $F$  is the force acting on the system and  $L$  is the length of the contact line, so the width of the gear.  $R'_x$  is the effective radius in the direction of  $b$ , determining the contact area. In the direction of  $L$ , both surfaces are flat so the contact will have length  $L$ .  $E'$  is the effective modulus of elasticity.

The effective radius is:

$$\frac{1}{R'_x} = \frac{1}{R_{x,1}} + \frac{1}{R_{x,2}} = \frac{1}{d/2} + \frac{1}{D/2} = \frac{1}{R_{x,1}} \quad (2)$$

In which  $R_1$  is the radius of the pinion and  $R_2$  is the radius of the rack. Both are half the radii,  $d$  and  $D$  of the pinion and rack respectively as shown in Figure 2.3. The radius of the pinion is the radius of curvature at the pitch. The rack has straight teeth, so the radius is  $\infty$ .

The effective modulus of elasticity is:

$$\frac{1}{E'} = \frac{1}{2} \left( \frac{(1 - \nu_1)^2}{E_1} + \frac{(1 - \nu_2)^2}{E_2} \right) \quad (3)$$

In which the Poisson ratio ( $\nu$ ) and E-modulus ( $E$ ) are material properties of the pinion and rack contacting materials.

The mean pressure  $p_m$  is calculated using the relation between pressure and load, where the contact area is  $2bL$ :

$$F = p_m A = 2p_m bL \quad (4)$$

The relation between the maximum pressure  $p_{max}$  and mean pressure is:

$$p_{max} = \frac{4}{\pi} p_m \quad (5)$$

Rearranging Equation 1, and applying Equation 4 and Equation 5, leads to the maximum contact pressure in a line contact situation.

$$p_{max} = \left( \frac{F}{L} \frac{E'}{\pi R'_x} \right) \quad (6)$$

### 2.3 Lubrication

The main functions of lubrication are to reduce friction and wear by separating the surfaces or creating a protective boundary layer (or a combination of both) such that the surfaces of the bodies do not touch.

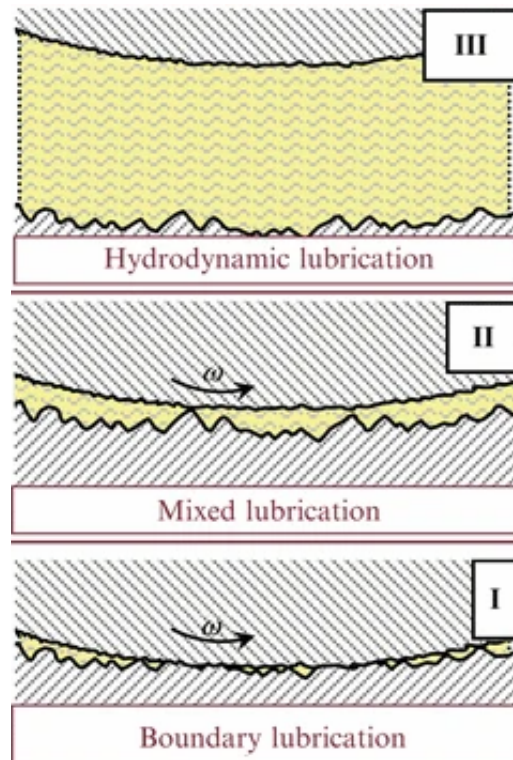


Figure 2.5: Lubrication regimes [10]

Based on the characteristics of grease base oils, boundary lubrication is expected and grease consists of additives that create boundary lubrication. By reducing friction with boundary lubrication, the grease cools the contact (as the bulk does not touch (as much)). As seawater is present in offshore applications, it is required to keep this out. Grease can do this job very well, especially offshore greases, that are highly water resistant [1]. It also can protect against foreign hard particles.

The lubrication regime of a system can be calculated using the Dowson-Higginson equation to calculate the film thickness in a line contact [11]. This equation is still used as a design rule in lubricated systems [12]. These calculations estimate that the base oil alone is the determining factor. In grease, other properties can influence the film thickness next to the base oil viscosity so the real values in greased systems can be different [13].

$$H^* = 1.6G^{0.6}U^{0.7}W^{-0.13} \quad (7)$$

Where  $H^*$  is the dimensionless minimum film thickness for a line contact which can be expressed in the minimum film thickness  $h_{min}$  and the reduced curvature in x-direction  $R'_x$  as calculated in Equation 2:

$$H^* = h_m / R'_x \quad (8)$$

So:

$$h_m = 1.6G^{0.6}U^{0.7}W^{-0.13}R'_x \quad (9)$$

Where the dimensionless material parameters  $G$ , dimensionless speed  $U$  and dimensionless load  $W$  are calculated as shown in Equations 10, 13 and 17.

$$G = \alpha \cdot E' \quad (10)$$

$E'$  is calculated the same way as in Equation 3. The viscosity pressure coefficient  $\alpha$  can be calculated as shown in Equation 11, based on ISO standards [14].

$$\alpha = 10^{-6} \cdot 0.1122 \cdot \nu^{0.163} \quad (11)$$

Where  $\nu$  is the kinematic viscosity,  $\eta$  is the dynamic viscosity at ambient pressure and  $\rho$  is the density of the base oil.

$$\nu = \frac{\eta}{\rho} \quad (12)$$

$$U = \frac{\eta_0 \cdot v_e}{E' \cdot R'_x} \quad (13)$$

Where  $v_e$  is the entrainment speed which can be calculated by:

$$v_e = (v_1 + v_2) / 2 \quad (14)$$

To be able to determine the viscosity for different temperatures than the given data by grease suppliers, an additional step is required. Reynolds suggested an equation that is commonly used to calculate the viscosity when 2 states are known, but the required state is unknown [3]

$$\frac{\eta}{\eta_0} = e^{-\beta(T-T_0)} \quad (15)$$

Where  $\eta$  is the previously shown dynamic viscosity at ambient temperature  $T$ .  $\eta_0$  is the reference viscosity at a reference temperature  $T$ .  $\beta$  is the temperature coefficient that is calculated by interpolation between two reference points with temperatures  $T_{min}$  and  $T_{max}$  and corresponding viscosities  $\eta_{T_{min}}$  and  $\eta_{T_{max}}$ :

$$\beta = \frac{-1}{T_{max} - T_{min}} \ln \frac{\eta_{T_{max}}}{\eta_{T_{min}}} \quad (16)$$

$$W = \frac{w_z}{E' \cdot R_x'^2} \quad (17)$$

With the minimum film thickness known, a film parameter  $\Lambda$ , which is used in engineering practice, can be calculated and by this, the lubrication regimes in the Stribeck curve can be determined [15].

$$\Lambda = \frac{h_m}{\sqrt{RMS_1^2 + RMS_2^2}} \quad (18)$$

Where RMS (Rq or Sq) is the root mean square roughness.

In Figure 2.6, the lubrication types for a certain  $\Lambda$  value can be seen with the corresponding coefficient of friction behaviour. The lubrication type will be boundary lubrication if  $\Lambda < 1$ , mixed lubrication

if  $1 \leq \Lambda \leq 3$  or (elasto)hydrodynamic lubrication if  $\Lambda > 3$ . In (elasto)hydrodynamic lubrication, the fluid is carrying the load. In boundary lubrication, the surface is carrying the load with boundary layers. Mixed lubrication is a combination of both.

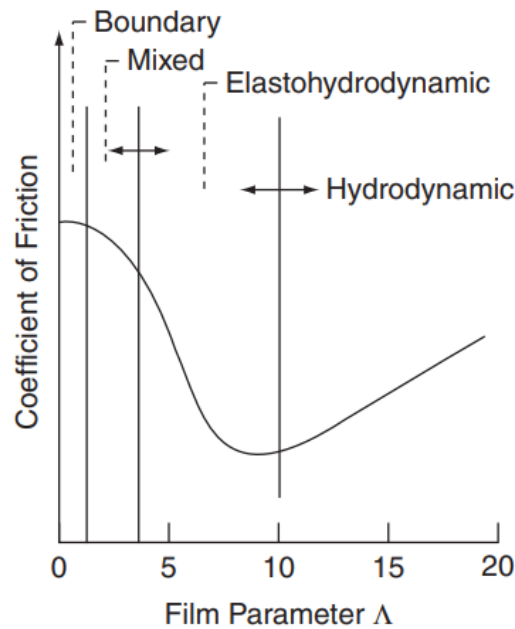


Figure 2.6: Stribeck curve: Coefficient of friction versus film parameter  $\Lambda$  with a corresponding lubrication regime[15]

## 2.4 Friction

Friction is connected to the efficiency of a system of rubbing surfaces. Reducing the coefficient of friction (COF) leads to increasing efficiency. The classical friction laws hold for metals. Generally, the friction coefficient is the friction force (force required to move a component) divided by the normal force:

$$\mu = \frac{F_f}{F_n} \quad (19)$$

Mathematical models cannot completely predict friction, however, their insights can be used to manage (and thus reduce) friction [3]. Generally, friction consists of a combination of a ploughing and adhesive component, where the contribution of both can vary. Each of the two will be explained on the next page.

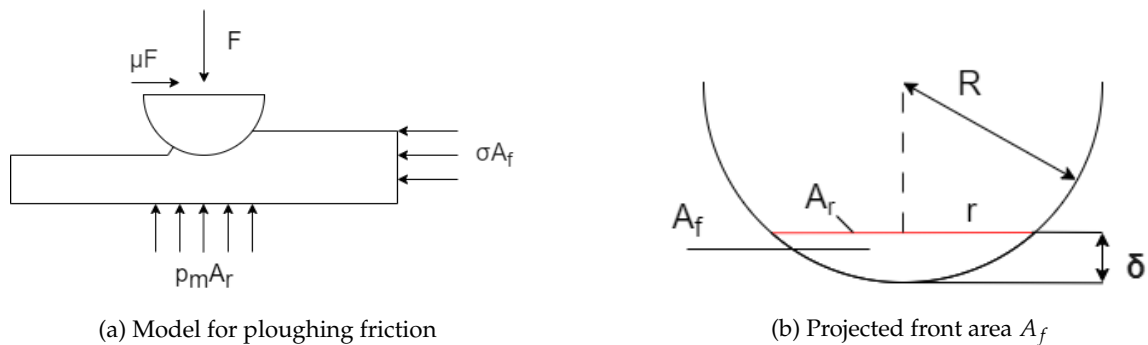


Figure 2.7: Model for ploughing friction and projected front area reproduced from [3]

For ploughing friction, the following holds [3]. When the hardness difference is bigger than 20%, the harder surface can penetrate the softer surface. Hard particles, metal debris or dust can contribute to this. This is called ploughing. During a sliding motion,  $F$  and  $p_m A_r$  are in balance, with  $p_m$  being the contact pressure and  $A_r$  being the real contact area. The friction force is equal to  $\sigma A_f$ .  $A_f$  is the projected front area, a circle segment, and  $\sigma$  is the average stress. The coefficient of friction by the ploughing component  $\mu_p$  is:

$$\mu_p = \frac{\sigma A_f}{p A_r} \quad (20)$$

When plastic deformation is present during ploughing, both  $\sigma$  and  $p_m$  approach the plastic deformation resistance [16]:

$$\frac{\sigma}{p} \approx 1 \quad (21)$$

$$\mu_p \approx \frac{A_f}{A_r} \quad (22)$$

This function can be seen as a function of the penetration depth  $\delta/R$ .  $\mu_p$  increases with dimensionless penetration depth. The ploughing friction can be reduced by [3]:

- Applying a high hardness on both surfaces. This results in a low penetration depth  $\delta$  as in Figure 2.7b.
- Applying a low roughness on the hard surface. This results in a large asperity radius  $R$  as in Figure 2.7b, due to its big wavelength
- Using lubrication to separate surfaces (but this will be eliminated as a goal of this project)

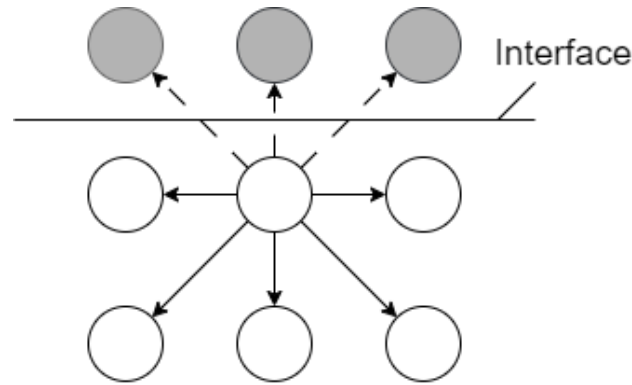


Figure 2.8: Atomic interactions causing adhesion between material 1 (white) and material 2 (grey), reproduced from [3]

Adhesive friction is present due to atomic interaction, see Figure 2.8. The friction force has a shear strength  $\tau$ , that needs to be broken. This can be the shear stress that leads to adhesive bond breakage between both surfaces or the cohesive strength of the soft surface. This  $\tau$  is proportional to the real contact area. So:

$$F_f = \tau A_r \quad (23)$$

And thus:

$$\mu_a = \frac{\tau A}{N} \quad (24)$$

For a normal load,  $F = p_m A_r$ . During plastic deformation  $p_m$  is equal to hardness  $H$  so the friction by adhesion is:

$$\mu_a = \frac{\tau}{H} \quad (25)$$

Adhesive friction can be reduced by [3]:

- Using lubrication to separate surfaces (but this will be eliminated as a goal of this project)
- Using dissimilar materials. This leads to weaker bonds. For example, alloys can help with this. Besides, they reduce surface energy  $\gamma$  and increase hardness  $H$
- A high roughness. With a smooth surface, a high real contact area is present, leading to more atomic bonds and thus more adhesion.
- Reducing surface energy  $\gamma$ . Done by increasing hardness  $H$ :  $\gamma = CH^{1/3}$  [17]. Besides, high hardness leads to a low  $A_r$ .
- Using non-metals, however, this is not usable in this project due to the high contact pressure present.
- Metal oxides to prevent pure metallic contact and increase hardness.

## 2.5 Wear

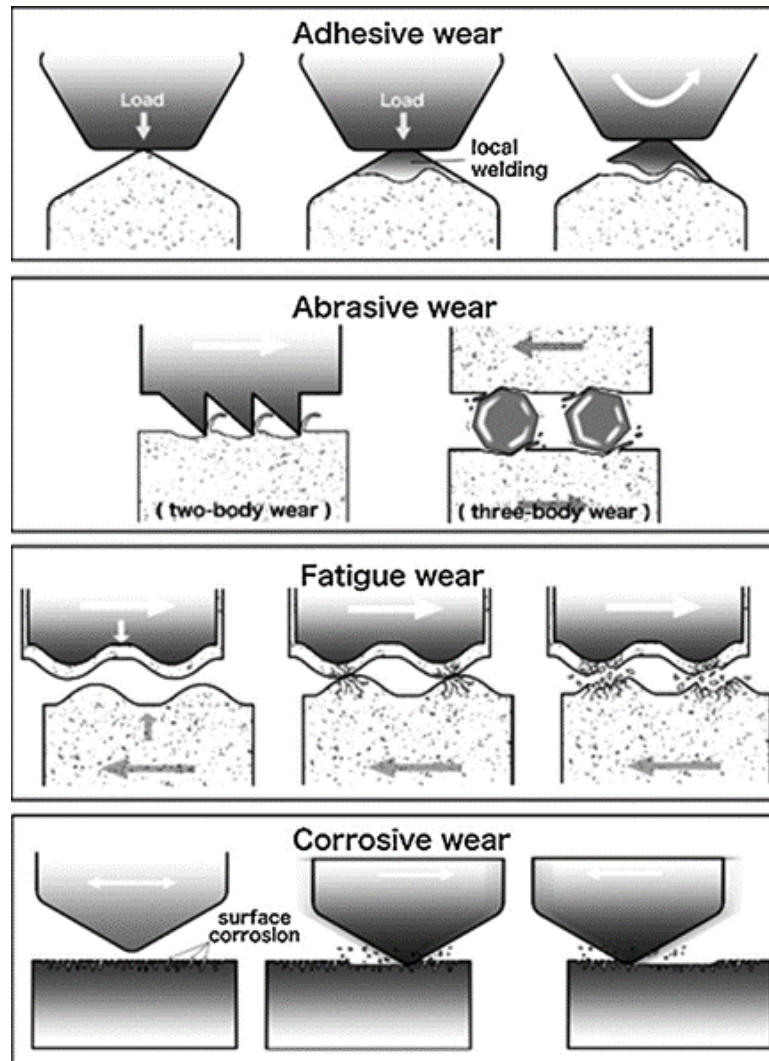


Figure 2.9: 4 main types of wear [18]

Wear is the main limitation for the technical and economic service life of a machine [3]. Performance is limited by wear and clearances are forming due to material removal. In other words, wear is connected to reliability and lifetime. There are 4 main types of wear: Abrasive wear, adhesive wear, surface fatigue and corrosion[3].

- Adhesive wear: Due to strong adhesive bonds as discussed in friction, local welding can be present. In movement, this results in material shearing off and this leads to transfer that can be temporary (free wear particles) or permanent. adhesive wear can be very mild, however, in machines it can be so serious it stops the machine from being usable. Specific forms are:
  - Scuffing: If the critical temperature of a lubricant is reached, this will fail and local welding will take place. Generally, this is prevented by antiscuffing (EP) additives.
  - Cold welding and galling: With metallurgical comparable materials, rubbing with sufficient force. Cold welding (galling) can take place. This can create a bond strength as strong as the bulk material. Galling is usually associated with poor lubrication and a high force with low velocity. It can ruin a surface in one pass.

Adhesive wear can be reduced or prevented in the same way as adhesive friction.

- Abrasive wear: This can be present in two modes, two-body and three-body abrasive wear. In two-body abrasive wear, the hard asperities plough into the soft material, leading to scratching/ploughing or polishing. In three-body abrasive wear, hard particles are embedded in the soft material, leading to the opposite of two-body abrasion and wearing the hard surface. The hard particles can come from the environment as well from hard wear particles that are not removed from the contact. The ways to reduce ploughing friction also apply to abrasive wear. Additional applicable ways to reduce ploughing wear are: reducing the hardness difference of the surfaces to <10%, however, this could increase adhesive wear (cold weld/galling) under high load. The removal or prevention of hard external and wear particles (hardening, oxidation particles, environmental particles) will remove possibilities for three-particle abrasion.
- Fatigue wear – This is the dominant wear mechanism in rotating mechanisms (possibly in combination with slip). Repeated stress-strain events lead to crack initiation, propagation and detachment of fatigued material. This can lead to pits (small in size) and spalls (big in size). Micropits can form the same way (possibly with corrosion). These can either be removed if slip is present and this can run in, otherwise, they will grow. Rolling contact fatigue can be reduced by a low contact pressure, leading to less stress. Besides, high hardness has a high load rating and low roughness can be used to reduce the possible starting points of crack initiation. At last, case hardening can be used to create compressive stresses in the material, reducing the chance of crack initiation. This method is used in many current used gear systems.
- Corrosive wear: This is due to complex thermodynamical reactions leading to material removal. This can be either wear-resistant or wear-increasing. The oxidation layers protect the surface from wearing down in sliding wear and can be used as a lubricant [19][20] [21]. It is, however, not always sure that the oxidation layer has enough time to be effective in protection [22]. Another factor is the bond strength of the oxide layers which needs to be big enough to be able to act wear-resistant [19]. Oxidation is a difficult process that in combination with wear is less understood and very case-specific. Several studies have been done on the effect of oxidation to wear. Generally in steel, a few types of corrosion are dominant. For temperatures below 560 °C, Hematite ( $Fe_2O_3$ ) and magnetite ( $Fe_3O_4$ ) can be formed [23], along with  $FeCr_4$  and  $Cr_2O_3$  when Chromium is present.  $Fe_3O_4$  and  $FeCrO_4$  are known to be protective oxides [24][25]. The other 2 are associated with severe wear. The wear will be lower if the film is regrown. Only the oxide layer will wear down in that case, in a mild way as can be seen in figure Figure 2.10. This oxide layer is usually very thin and difficult to observe. If the layer is too weak, intense corrosion can happen if all of the oxides are removed resulting in an exposed surface. this can also happen in cracks or fissures, as can be seen in figure Figure 2.10. In this case, corrosion increases wear as intense corrosion happens.

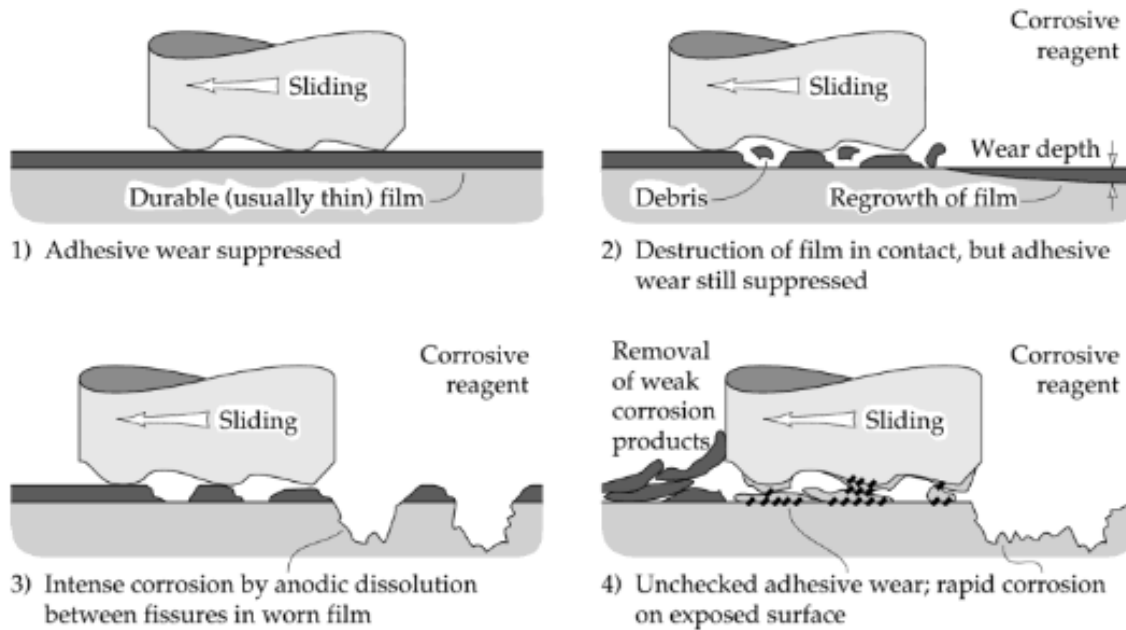


Figure 2.10: Oxidative wear types[24]

The Archard wear equation can be used to describe the wear volume [26]:

$$V = k \cdot F \cdot s \quad (26)$$

Where  $F$  is the load and  $s$  is the sliding distance. The specific wear rate  $k$  ( $mm^3/Nm$ ) is a very useful tool to compare the wear of materials as the volume loss is normalised over the load and sliding distance.

This is used widely in tribological experiments [27]. It is very easy to compute, however, its drawback is that  $k$  is very system-dependent. Each system can be very different so  $k$  needs to be determined experimentally. Originally it was derived from adhesive wear, but it is used for abrasive wear and other types of wear too (for example abrasive). In [28], the derivation is described:

On every instance during the contact, the true contact area  $A_t$  is

$$A_t = \sum_n \Delta A_t = n \Delta A_t \quad (27)$$

With:

$$A = \frac{F}{H} \quad (28)$$

It follows that:

$$n = \frac{1}{\Delta A_r} \frac{F}{H} \quad (29)$$

A constant load carrying capacity is present when every asperity contact is changed by a new one, with the same characteristic after its effective carrying distance  $d$  (as can be seen in Figure 2.11). At  $n$  simultaneous contacts, the total contacts per sliding distance is:

$$N = \frac{n}{d} = \frac{1}{\Delta A_r d} \frac{F}{H} \quad (30)$$

Of these contacts a fraction  $\kappa$  (transfer probability) leads to material transfer, where a volume  $\Delta V = A_w h$  is transferred. Where  $h$  is the mean height of a transferred particle. The transferred material

volume per unit of the sliding distance is:

$$\frac{dV}{ds} = \kappa N \Delta V = \kappa \frac{hF}{Hd} \quad (31)$$

The total transferred volume after sliding distance  $s$  is found by:

$$V = \kappa \frac{hFs}{Hd} \quad (32)$$

In quasi-stationary equilibrium, the transferred material is equal to the formation of free wear particles. If that is not the case, the transfer layer will grow and the system will not in equilibrium. So  $V$  in Equation 32 is the total volume removed by adhesive wear. Equation 32 and Equation 26 combined result in a relation between  $k$  and  $\kappa$

$$\kappa = kH \frac{d}{h} \quad (33)$$

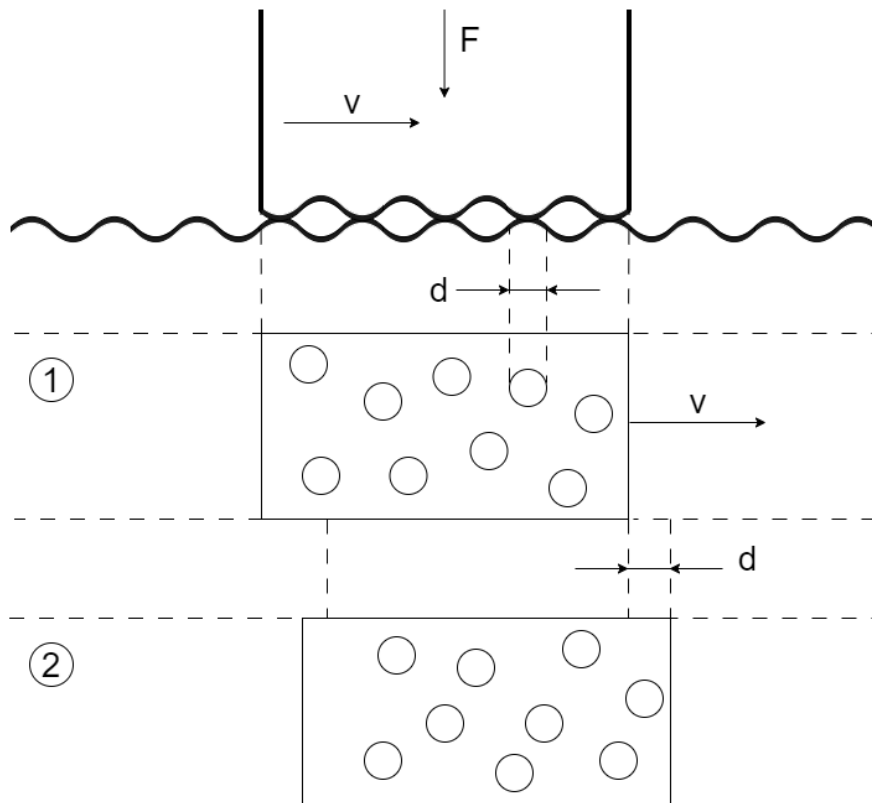


Figure 2.11: Archard model, reproduced from [28]. Loads are carried by the circular asperities, with diameter  $d$ . After sliding distance  $d$ , the situation moves from situation 1 to situation 2, and the asperities are changed by new ones.

Wear will have a running-in period that is a transient state. This trajectory is very unpredictable, as wear gradually decreases over time. It is experimentally determined that after some time the wear process stabilizes and a linear relation between sliding distance and worn volume follows [28]. To determine the actual lifetime of a mechanism, wear needs to be measured multiple times with a

time interval in between [29]. The final linear situation can be extrapolated. In literature, however, the false expression in Figure 2.12 is used many times. This saves measuring time and if the time (exposure to wear) is large enough, it is approximated quite well with some overestimation when extrapolated. However, only momentarily it can be predicted accurately.

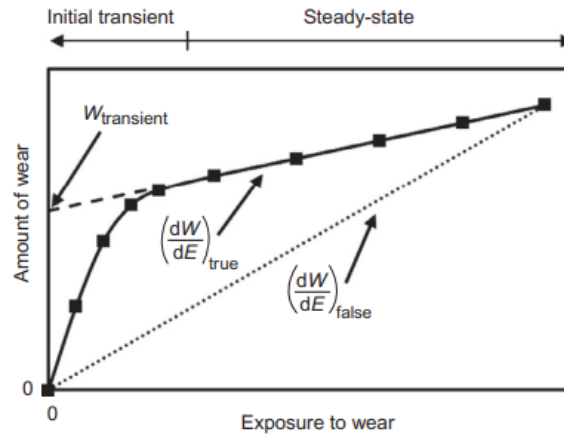


Figure 2.12: Steady state of wear [29]

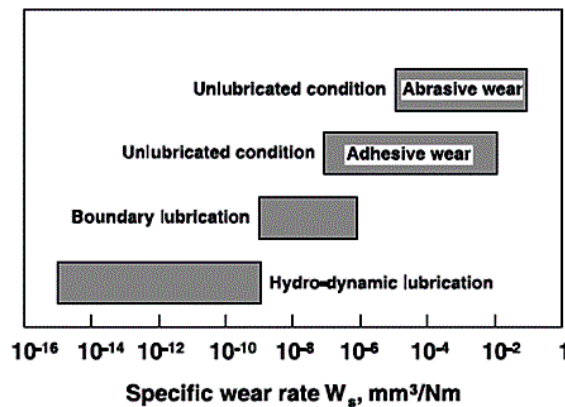


Figure 2.13: Typical wear mechanisms for certain wear rates[30]

Figure 2.13 shows the general wear regimes wear can act in. However, these are regimes and some cases might vary from this as wear is very system-specific. Tribological systems can easily vary as is explained in Figure 2.1.

## 2.6 Gear kinematics and tribology

Gears have a combination of rolling and sliding present with connected characteristics. This will be explained here. Within gears contacts, the line on which the teeth are in contact, the line of action is determined by the pressure angle. This line is the common tangent of the base circles [31]. This line starts at the start of active profile (SAP) and ends in the end of active profile (EAP). See the red line in Figure 2.14

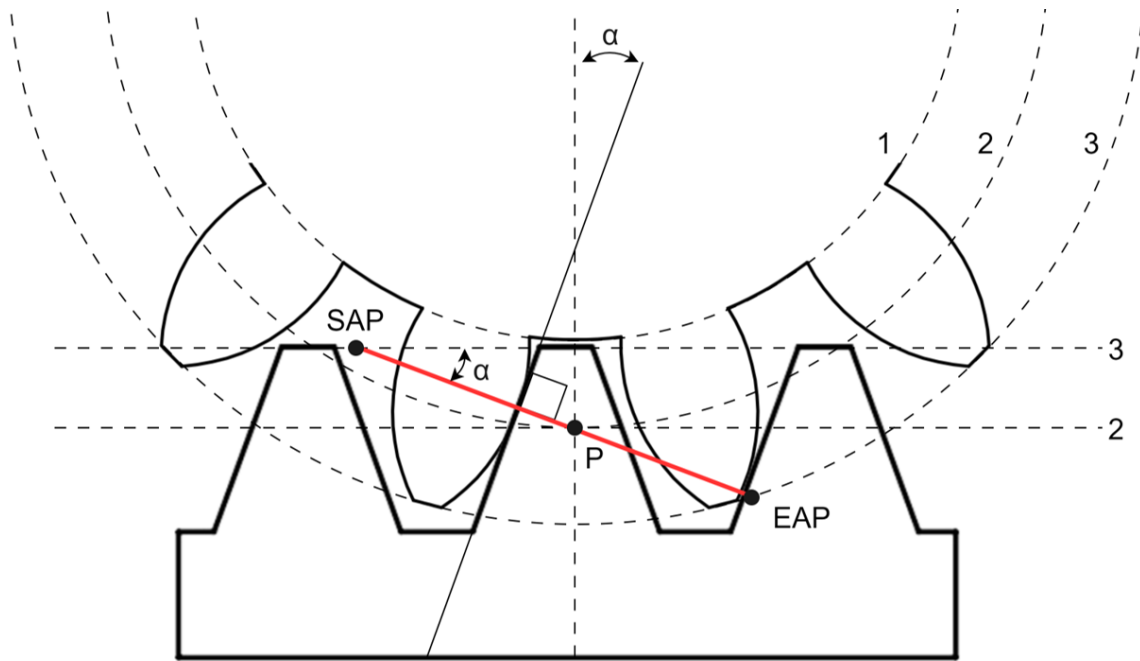


Figure 2.14: Based on [31], 1 = root diameter, 2 = pitch diameter, 3 - tip diameter,  $\alpha$  = pressure angle

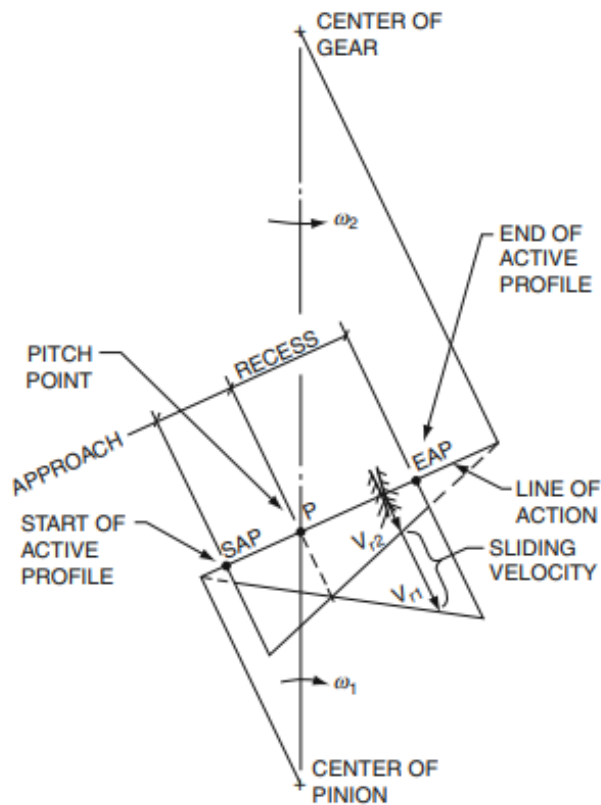


Figure 2.15: Rolling and sliding velocity of a pinion-gear system [32]. This will be similar except for an infinite radius of the rack for a rack-pinion system.

The Line of action is also shown in Figure 2.15.  $\rho$  is the transverse radius that changes as the gear

rotates and thus the contacting point changes. Based on this radius and the known angular velocity of the gear  $\omega$ , the velocities of the rack and pinion can be calculated. For a rack and pinion, the following holds:

$$v_{ri} = \omega_i \cdot \rho_i \quad (34)$$

However, the rack tangential velocity ( $v_{r2}$ ) is the same as the tangential velocity of the pinion at the pitch point ( $v_{r1}$  @P) over the whole line of action. This is the case because a rack is in linear motion and a continuous motion is assumed. This is not the case if  $v_{r2}$  was not continuous.

$$v_{r2} = v_{r1}@P \quad (35)$$

And for 1:

$$v_{r1} = \omega_1 \cdot \rho_1 \quad (36)$$

The sliding velocity is determined by the difference in velocity between both bodies, resulting in slip.

$$v_{s1} = v_{r1} - v_{r2} \quad (37)$$

Because both gears rotate in a different direction (clockwise and anticlockwise):

$$v_{s2} = -v_{s1} \quad (38)$$

The entertainment velocity  $v_e$  is used to calculate the slide-to-roll ratio SRR and is calculated as explained in Equation 14.

$$SRR(\%) = \frac{v_{s1}}{v_e} \quad (39)$$

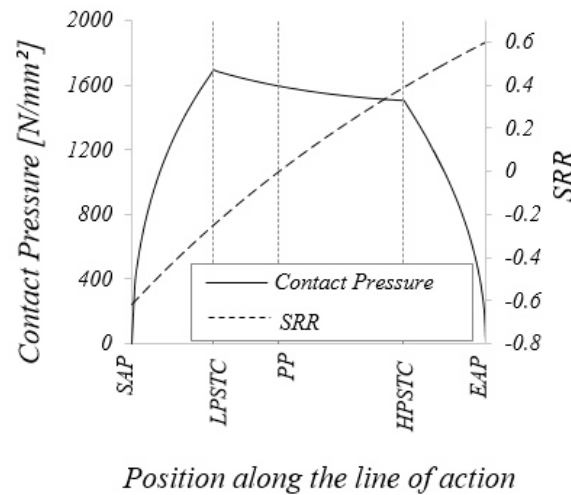


Figure 2.16: Example of SRR and pressure development over the rotation of the gears. [33]

Above, an example of the SRR and pressure development over the rotation can be seen over a full rotation (from SAP to EAP). Slip results in sliding surfaces while rolling is present (and thus SRR) and can result in wear, as is explained in the Archard wear equation, when asperities slide over each other. During pure rolling no slip is present, and thus theoretically no wear. This is at the pitch point P (or PP as shown in Figure 2.16) where the tangential velocities are the same. LPSTC is the lowest point of single-tooth contact and HPSTC is the highest point of single-tooth contact. One tooth pair contact is present between these two points, while two or more are outside these two points. The

positions of these points vary with the distance the rack and pinion are mounted from each other. If this distance is low, LPSTC and HPSTC are close to each other. A low distance can result in always having minimal two gears in contact and in that case, LPSTC and HPSTC are not present.

In Figure 2.17, can be seen how slip is acting around the pitch for a rolling and sliding contact. The resulting wear can be seen in Figure 2.18, where the pitch is unworn and around this. Slip has created a wear pattern that is maximum at the maximum slip. Rolling theoretically cannot cause sliding wear but can cause rolling contact fatigue. In a gear system, a combination of both sliding and rolling can be present, which changes as SRR changes over the angle of gear rotation as can be seen in Figure 2.16.

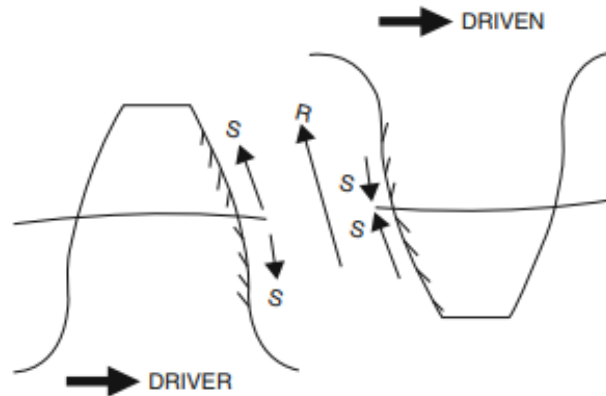
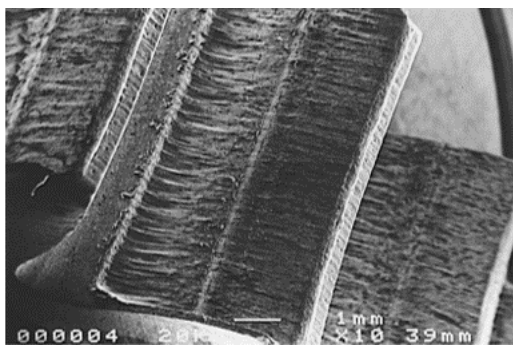
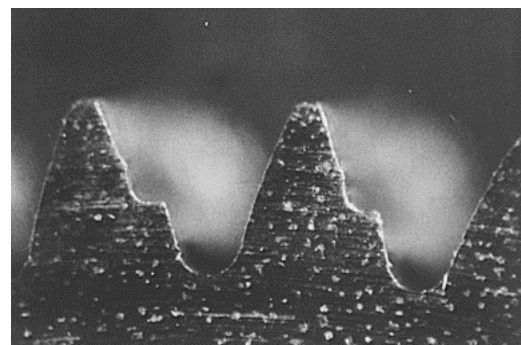


Figure 2.17: Rolling and sliding directions of a pinion-gear system [32]. Engagement of the gears is at the surface with the dashed lines. For a rack-pinion system, this will be similar except for an infinite radius (straight line) of the rack.



(a) Top view



(b) Side view

Figure 2.18: Visualisation examples of the wear profile of a gear. This profile is of an unlubricated 1 mm module SG iron, driven gear after 300 h at 3Nm and 500 rev/min.[34]

## 2.7 Possible solutions

The goal of this project is to find a solution for greased open gear systems. One of the possible solutions is to create a coating that reduces friction and wear. 3 possible coating types are found with their properties summed up in Table 1.

Table 1: Three possible solutions for greaseless open gears with their properties [35] [36][37] [38]

	APS	PTA	Laser Cladding
<b>Heat Source</b>	Gas Flame/ Plasma	Plasma/Electric Arc	Laser Beam
<b>Coating Thickness</b>	0.1-2.5 mm	1-6mm	0.5->4 mm
<b>Bond Type</b>	Mechanical	Metallurgical	Metallurgical
<b>Bond Strength</b>	<80 MPa	<800 MPa	<800 MPa
<b>Porosity</b>	2-5%	100% dense	100% dense

PTA and laser cladding are almost similar processes and are superior to APS as they produce a much stronger metallurgical bond than the mechanical bond. Besides a thicker coating can be achieved, which increases the allowable wear. In PSA porosity is present, which can lead to brittle behaviour. Höganäs suggested not to use PTA, as the offshore pinions are difficult to handle. Handling and accessibility are better with laser cladding due to the focusing of the laser beam. Besides, a lower heat input reduces distortion and heat-affected zones when using laser cladding over PTA. Laser cladding is based on this found to be the best solution.

### 2.7.1 Laser cladding

Laser cladding works by a powder or wire feed that is melted by a laser source as can be seen in Figure 2.19. It is a type of additive manufacturing and/or coating. The low heat input and rapid solidification create a very good grain refinement in the coating used [39]. This results in a high-strength coating. Dilution between the cladding and the workpiece (substrate) creates a strong metal bond. The adhesive strength of these coatings with this process can (when the steel substrate is preheated) be better than the cohesive strength of the steel [40]. Preheating is required, to reduce adhesive stresses in the heating affected zone resulting from different thermal expansion of the coating and substrate. These stresses can result in the cracking of the cladded coating.

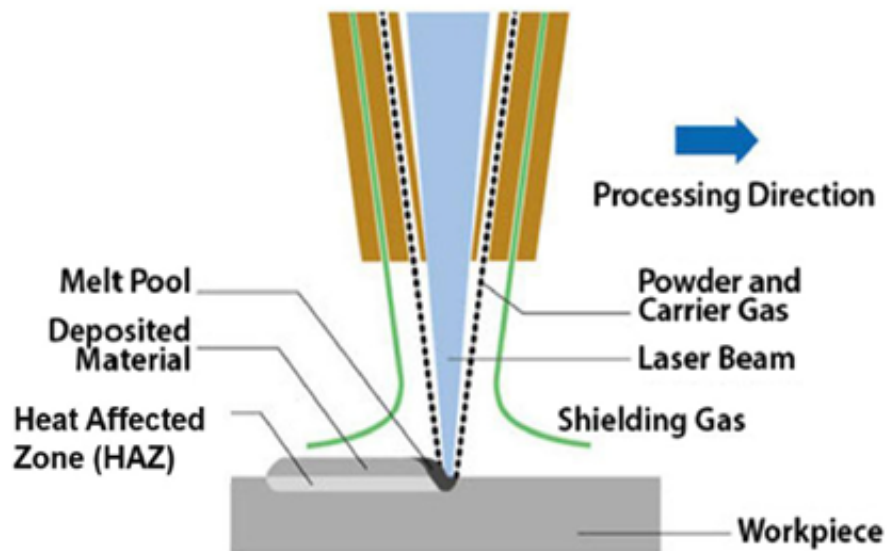


Figure 2.19: Schematic presentation of the laser cladding process [39]

### 2.7.2 Possible laser-cladded coatings

The coating of the rack-pinion system will be applied on the pinion as this makes the most cycles and thus is wanted to have the least wear. This coating may not be brittle and requires good friction and wear properties as a combination of rolling and sliding is present in combination with a high load. This makes many coating materials unfeasible. The proposed laser-cladded coatings for this research are cobalt-based superalloys. These are known to have low friction and wear [6][7]. However, these parameters are dependent on the system and its properties. Typically cobalt-based superalloys also have a high hardness and high temperature resistance [41]. The material is ductile and has a good bonding strength to metals so the high loaded situation forms no problem. The possible laser-cladded coatings are Stellite 21, Stellite 6, Stellite 190 and Tribaloy T-400. Additions of Cr, C, W and/or Mo to the cobalt matrix result in resistance to cavitation, corrosion, erosion, abrasion and galling, however, again this is very case-specific.

#### **Stellite 21**

The properties of stellite 21 are very much dependent on its processing technique [42]. It consists of a CoCr matrix with hard carbides in it. It is the softest of the coatings with a possible hardness of (290 - 430 HV) [42]. It has the best corrosion resistance and worst hard particle abrasion resistance of the stellite family [6]. Its wear rates and friction coefficient based on literature compared to other coatings (non-stellites) and untreated steel sliding against steel are found to be very good and promising [43].

#### **Stellite 6**

Stellite 6 is the most widely used stellite type [44]. It also has a CoCr alloy matrix with hard carbides, however, more than stellite 21 so the hardness is higher, depending on the production method (380 - 490 HV). Its wear rates and friction coefficient based on literature compared to other coatings (non-stellites) and untreated steel sliding against steel are found to be very good and promising [45].

#### **Stellite 190**

Stellite 190 has a very high abrasion resistance. It has the highest amount of carbides and the highest hardness (570-760 HV) [46]. Stellite 190 is corrosion-resistant in mildly oxidizing environments, the worst of the selected materials. Its wear rates and friction coefficient based on literature compared to other coatings (non-stellites) and untreated steel sliding against steel are found to be very good and promising. Besides in this particular literature, stellite 190 shows better abrasive resistance than stellite 6 [47]. It is not against the same type of steel, so this comparison is not true for this research. However, it tells something about the relative abrasion resistance.

#### **Tribaloy T-400**

During production, this material showed cracks so it was not possible to achieve a suitable surface and shape for the experiments. Further elaborations on why it cracked are in Appendix A. This means Tribaloy T-400 is not possible to experiment on, leaving the different stellites as possible coatings

The reason it was intended to perform experiments on Tribaloy T-400 is its outstanding resistance against wear, galling and corrosion [7]. Tribaloy consists of intermetallic phases that are very hard, called laves. It is a bit softer than stellite 190 but harder than stellite 6 (490-746). Its wear rates and friction coefficient based on literature compared to other coatings (non-stellites) sliding against steel are found to be very good and promising. Besides in this particular literature, Tribaloy T-400 shows better abrasive resistance than stellite 21 against 42CrMo4 in dry sliding [48].

For all coatings holds: no same tribological system (load, sliding velocity, environment) is experimented on in literature, so to know the differences and effects, experimental research is required.



### 3 Research questions

The main research question is composed based on the problem statement:

**To what extent are greaseless open gears feasible within the high-loaded systems in offshore applications?**

To answer this main question, it is supported by the following subquestions:

1. What are the current conditions in the used greased open gear systems?
2. What is the pure sliding wear behaviour of various coating solutions for a high load at a low speed, a medium load at a low speed and a medium load at a relatively high speed, under dry, seawater and pure water conditions?
  - (a) What is the influence of different types of lubrication?
  - (b) What is the influence of load?
  - (c) What is the influence of velocity?
  - (d) What is the influence of the hardness of the rack and the pinion material?



## 4 Current system properties

Many parameters of the systems were found in previous projects by Huisman. However, some data, for example, roughness parameters was extracted from technical drawings. Others had to be calculated based on theory.

### 4.1 Roughness

The roughness for all systems applied is found in technical drawings and can be found below. Some drawings, however, were unreadable or restricted.

Table 2: Roughness of rack and pinion in systems \*Exact value is unknown due to unreadable technical drawings, but this value is extracted from a similar pinion system

Application	Rack/pinion	Roughness Ra (micrometer)
Jacking system	Pinion	3.2 *
	Rack	500
Slew Bearing	Pinion	Not known
	Rack (outer ring)	1.6
Motion Compensated Pile gripper	Pinion	Not known
	Rack	1.6
Winch drive	Pinion	Not known
	Rack	3.2

### 4.2 Grease

2 different types of grease are used. Grizzly grease is used in the Jacking system and Castrol mollub is used in all other systems assessed in this thesis. Their properties are shown below:

Table 3: Type Grizzly Grease BIO 1-1000, NLGI 0-1 properties [1]

Type Grizzly Grease BIO 1-1000, NLGI 0-1	
Thickener	Calcium sulfonate complex soap
Base oil	Ester
Density, g/cm <sup>3</sup> 20	1.02
Base oil viscosity, mm <sup>2</sup> /s	
40 °C	1,000
100 °C	98
Biodegradability 28 days	>70%

Table 4: Castrol Molub-Alloy 936 SF Heavy properties [49]

Castrol Molub-Alloy 936 SF Heavy	
kg/m <sup>3</sup>	950
Base oil viscosity, mm <sup>2</sup> /s	
40 °C	2030
100 °C	57

### 4.3 Contact pressure

The theory in subsection 2.2 is used to calculate the exact contact pressures in the system. The inputs and following pressures are shown in Table 5. The inputs are either material properties of the used steels or system properties such as loads or lengths.

Table 5: Input parameters and results for maximum Herzian pressures  $p_{max}$ .

	$W/L$ (kN/m)	$R'_x$ (mm)	$E_1$ (GPa)	$E_2$ (GPa)	$\nu_1$ (-)	$\nu_2$ (-)	$p_{max}$ (Gpa)
<b>Jacking System</b>							
210 mm	42755.29	166.8	210	210	0.29	0.29	3.06
250 mm	35914.44	166.8	210	210	0.29	0.29	2.80
<b>Slew Bearing</b>	4250.00	67.7	210	210	0.29	0.29	1.51
<b>Motion Compensated Pile Gripper</b>	6987.20	67.7	210	210	0.29	0.29	1.94
<b>Winch Drive</b>	3687.50	65.7	210	210	0.29	0.29	1.41

### 4.4 Sliding velocity

This was already calculated by Huisman, based on Equation 37. For 5 points the corresponding input values are calculated and measured based on solidworks drawings. With these, the maximum value of the sliding velocity is found and the results are shown in Table 6.

Table 6: Sliding velocities in the systems

	<b>Max. sliding velocity (mm/s)</b>	<b>Entrainment speed <math>u_e</math> (mm/s)</b>
<b>Jacking System</b>		
210 mm	7.5	14.1
250 mm	7.5	14.1
<b>Slew Bearing</b>	80.0	240
<b>Motion Compensated Pile Gripper</b>	23.0	66
<b>Winch Drive</b>	459.0	1330

### 4.5 Lubrication regime

The lubrication regime is calculated for each system, using the theory in subsection 2.3 and the inputs in the tables above. The temperatures chosen are possible environmental situations.

Table 7: Lambda values for different temperatures

<b>Application</b>	$\Lambda$			
	<b>(-10°C)</b>	<b>(0°C)</b>	<b>(20°C)</b>	<b>(40°C)</b>
<b>Jacking System</b>				
210 mm	0.18	0.14	0.07	0.04
250 mm	0.19	0.14	0.08	0.04
<b>Slew Bearing</b>	4.09	2.54	0.98	0.38
<b>Motion Compensated Pile Gripper</b>	2.52	1.57	0.61	0.23
<b>Winch Drive</b>	6.81	4.23	1.64	0.63

Most operations are in the boundary lubrication regime, especially in summer conditions, when most of the offshore installation is done. It means that the surface is still in contact. This however as previously discussed, is only true for the base oil. For the complete grease other mechanisms can happen that change surface separation.

#### 4.6 Sliding distance

The sliding distance can be calculated by the integration of velocity, where the area is the total sliding distance. However, this is not possible in this case as the complete path of the velocity is unknown. Values for a few specific points (5) are known. The trapezoidal rule can be used to approximate this integration, using these specific points. Extra points are interpolated in between for extra accuracy:

$$\int_{t_0}^{t_n} v(t) dt \approx \frac{h}{2} \left[ v_0 + 2 \sum_{i=1}^{n-1} v_i + v_n \right] \quad (40)$$

Which can be calculated in Matlab by the 'trapz' command. The found sliding velocities are changed to absolute values (negative values are made positive). On the x-axis, time is plotted (which is known by the rotation velocity and rotating angle between SAP and EAP). The area under the graph in Figure 4.1 is the total sliding velocity between SAP and EAP (The sliding distance between entering and exiting the contact on 1 tooth in 1 rotation), graphically, the hatched lines in Figure 2.17. This can be seen in Table 8.

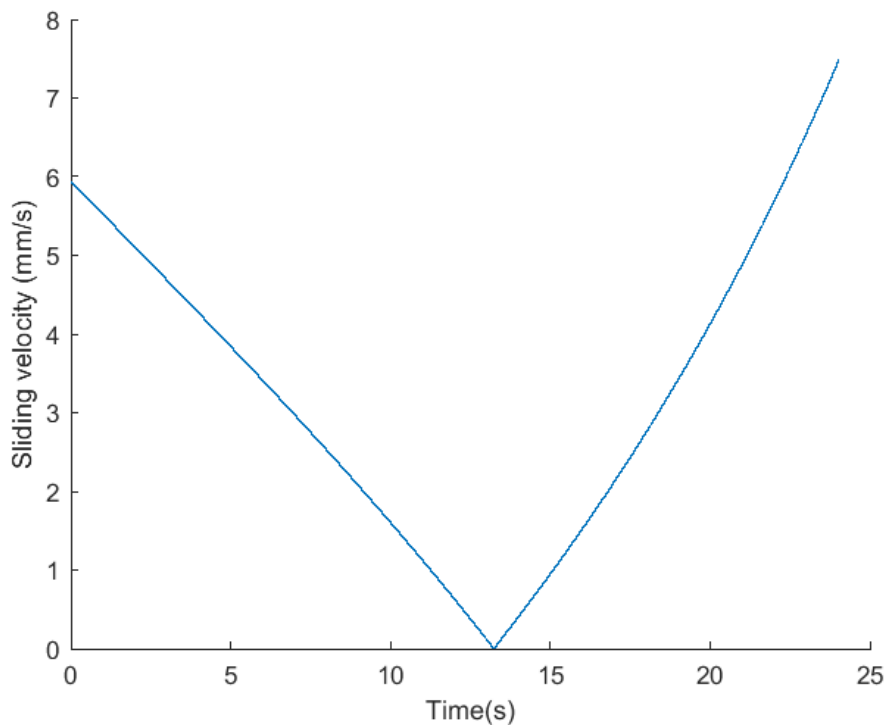


Figure 4.1: Absolute values of the sliding velocity per unit time

Table 8: Sliding distance for 1 tooth side per rotation

	<b>Jacking System</b>	<b>Slew Bearing</b>	<b>Motion Compensated Pile Gripper</b>	<b>Winch Drive</b>
<b>Sliding distance per cycle(mm)</b>	77.1528	27.7738	13.8869	27.1816

Multiplying this with the number of cycles (Table 9), results in the total sliding distance of 1 tooth during the service life of the gear, shown in Table 10.

Table 9: Number of cycles during service life

	<b>Jacking System</b>	<b>Slew Bearing</b>	<b>Motion Compensated Pile Gripper</b>	<b>Winch Drive</b>
<b>Cycles</b>	136180	1920001	2276277	5735215

Table 10: Sliding distance of 1 tooth during service life

	<b>Jacking System</b>	<b>Slew Bearing</b>	<b>Motion Compensated Pile Gripper</b>	<b>Winch Drive</b>
<b>Total sliding distance (m)</b>	10507	53326	31610	155892

## 4.7 Environment

The environment is a marine environment. Splash water and salt blowing in the contact in combination with water creates a highly corrosive environment. Besides, the systems are open so dust and other hard particles can enter if grease is not keeping this out sufficiently.

## 5 Experimental materials and methodology

### 5.1 Measurement inputs and materials

Pure sliding is experimented on the Universal Material Tester (UMT Tribolab) by Bruker [50]. The setup is shown in Figure 5.1, and a schematic of the setup that shows the process in detail is shown in Figure 5.2.

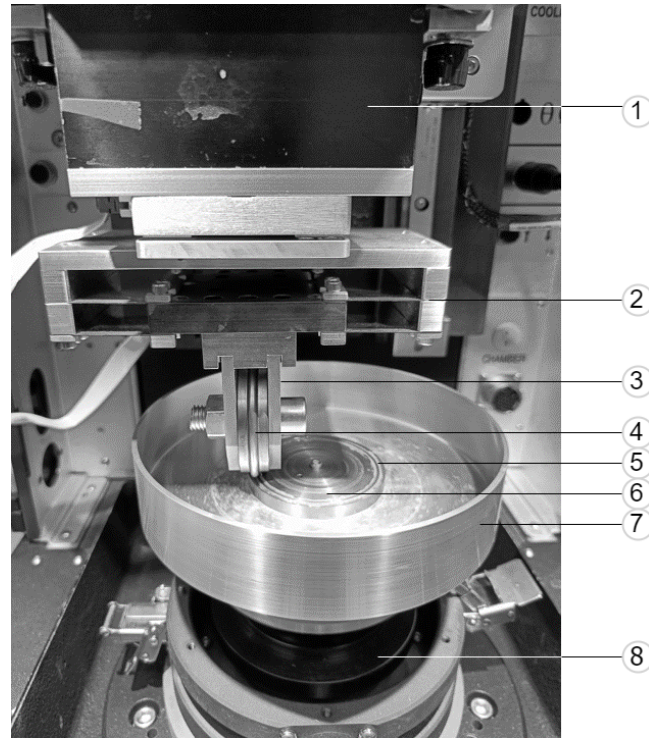


Figure 5.1: Setup for pure sliding. (1): Load cell, (2): Leaf spring assembly, (3): Clamp to fix the stationary disc, (4): (Cladded) stationary disc, (5): Wear track, (6): Rotating disc, (7): Water retaining cup and mounting mechanisms for the rotating disc, (8): Electromotor (rotating).

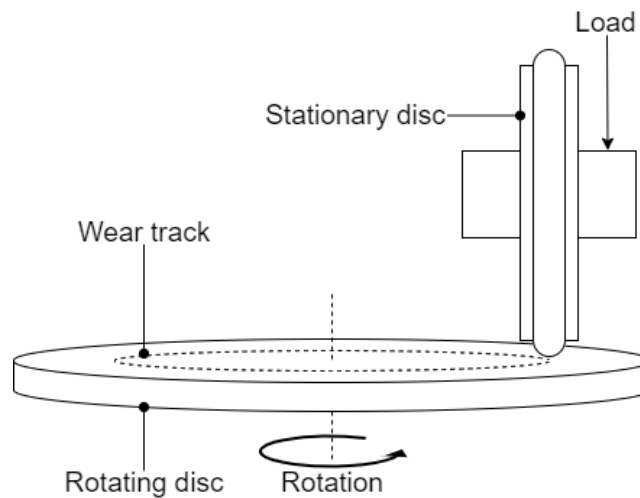


Figure 5.2: Schematic setup for pure sliding

A disc-on-disc experiment is performed. The top disc is stationary and is the pinion (cladded) material. This acts as a pin in a pin-on-disc experiment. However, to be able to achieve a high contact load, an elliptical or point contact was required. For machineability for laser cladding, an elliptical contact was chosen and thus a disc-on-disc with a radius in 2 directions (The surface is rounded off). The bottom disc acts as the rack material and is rotated by a rotating electromotor it is screwed onto. A normal load is applied by a load cell with a leaf-spring assembly in between to keep the normal load constant and account for height fluctuations of the rotating disc (due to roughness or a tilted surface). The water is kept in by a customised water retaining cup that is made of aluminium. Below, the dimensions of the samples can be seen. The stationary disc is turned on a lathe and the rotating disc is grinded to the specific dimensions.

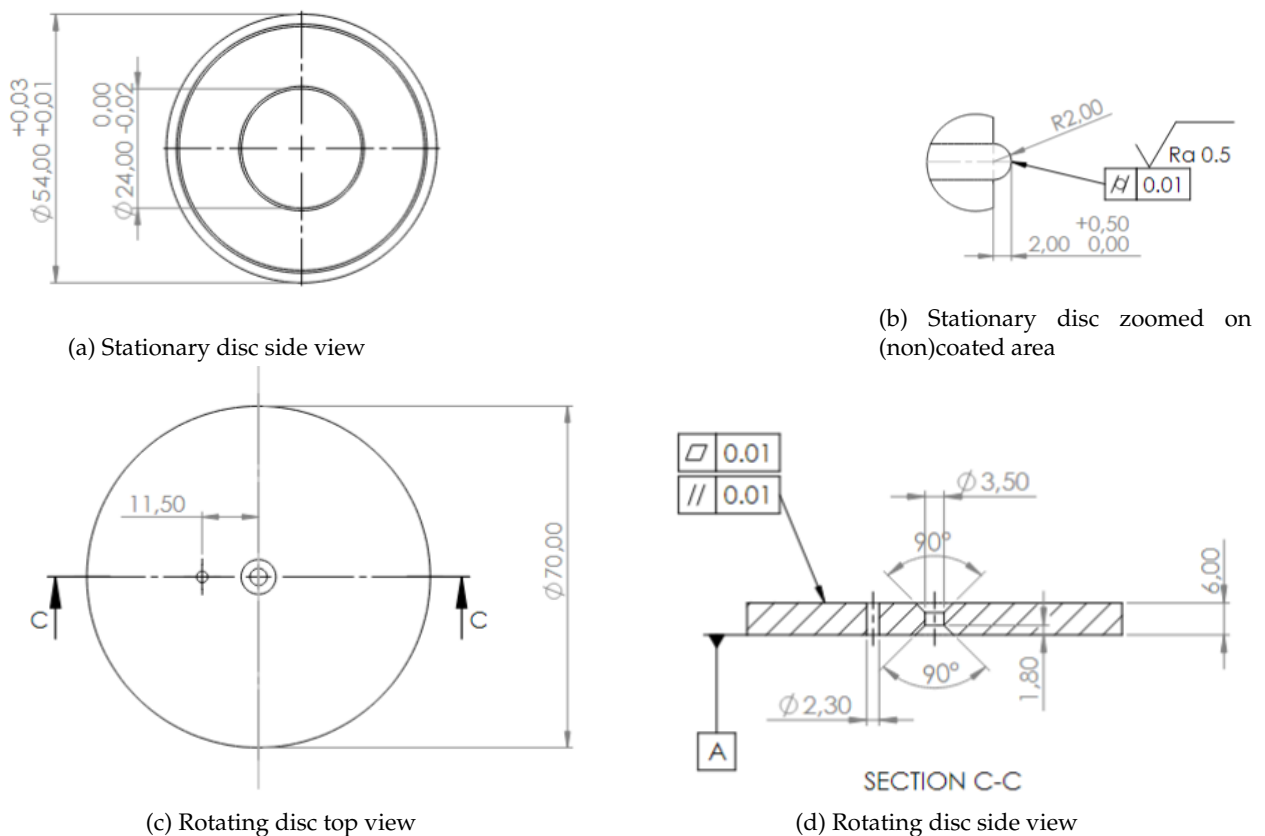


Figure 5.3: Part of technical drawings used to make the samples, already drawn before this thesis started by Huisman

### 5.1.1 Lubrication

The following lubricants are measured:

1. No lubrication
2. Grizzly grease (for properties see Table 3)
3. Q2 (pure) water which is a different name for type 2 water. This is produced using an Elix® Essential 3 Water Purification System from Merck Millipore Ltd. [51]. This system uses reverse osmosis (RO) to filter the water. A membrane is used that will block 99.5% of the ions, organics and salts while allowing water to pass through [52].

4. 3.5 wt. % sea salt solution of the salt shown in Table 11 mixed with Q2 water

Table 11: Minerals in the sea salt used to make a solution (g/100g)[53]

sodium chloride	calcium	magnesium	potassium	sodium
98.16	0.1	0.12	0.02	37.5

### 5.1.2 Materials

The coatings discussed in subsection 2.7.2 are researched, next to the current base pinion material. From the rack materials, 2 were found to have the same E-modulus and hardness. No additional value for the research question is found in examining both and only one is used (E690). This results in 2 rack materials: A hard and soft material (42CrMo4 and E690 respectively) with both the same E-modulus.

Table 12: Composition of rack materials (wt%), Fe is the base [54] [55]

	C	Mn	Si	P	S	Cr	Mo	Ni	V
<b>42CrMo4</b>	0.38-0.45	0.60-0.90	<0.40	<0.035	<0.035	0.90-1.20	0.15-0.30	-	-
<b>E690</b>	<0.21	<1.6	<0.5	<0.02	0.001	<1.5	<0.7	<3.5	<0.08

Table 13: Composition of pinion materials (wt%) [56][42][44][46][7]

	Base	Cr	W	C	Mo	Ni	Fe	Si	Mn	Others
<b>18CrNiMo7-6</b>	Fe	1.5-1.8	-	0.15-0.21	0.25-0.35	1.4-1.7		<0.4	0.5-0.9	-
<b>Stellite 21</b>	Co	26-29	-	<0.35	4.5-6.0	<3.0				Fe, Si, Mn
<b>Stellite 6</b>	Co	27-32	3-6	0.9-1.4						Ni, Fe, Si, Mn, Mo
<b>Stellite 190</b>	Co	27	14	3.3			<3			Ni, Si, Mo, Mn

All samples are turned to specifications

### 5.1.3 Cleaning

Before experimenting the samples are cleaned with isopropanol, after which the sample is dried with compressed air to not catch any particles when drying.

### 5.1.4 Hardness measurements

The hardness is measured for all used materials, with ZwickRoell DuraScan 70 G5 [57]. Before measuring, the samples are sawed through, embedded and polished. The rack materials (rotating disc) can be measured at the contacting surface as this is flat. The pinion disc, however, is round at the contacted surface which is difficult to measure as the hardness measurement is optical. a section of the disc is cut and embedded. The hardness is then measured as close to the surface as possible to have similar hardness as the surface hardness (the grey diamond in subsection 6.1)

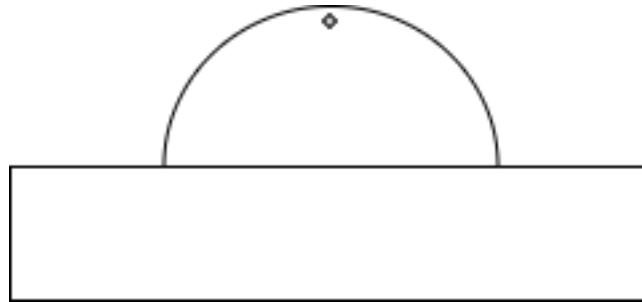


Figure 5.4: Hardness measurement spot on sawed and polished (cladded) pinion disc

The hardness measuring technique used is Vickers (according to ISO 6507) and the force used is 5 N, as the materials are hard.

### 5.1.5 Grouping of velocities and loads into experimental cases

Different pressures and velocities are present in the real contacts. The relevant pressures and sliding velocities are taken from Table 6 and Table 2 for each case. It is seen that the Jacking System is unique in terms of load and pressure. This results in case 1. The slew bearing and winch drive stand out in terms of velocity. These result in cases 3 and 4 with high velocities. It is chosen to round the velocities and pressures off to make them scalable. The Jacking system is close to 3 GPa, while all others are close to 1.5 GPa. For the velocities, it is chosen to take the values for cases 1, 3 and 5. It is chosen to make them 10 mm/s, 100 mm/s and 500. Many velocities are present for the low-loaded situation (1.5 GPa). To have a case that connects the high-loaded, low-velocity situation with the low-loaded, high-velocity situations, it is chosen to also measure case 2: a low-velocity, low-load case.

Table 14: Velocity and pressures per grouped case

Case	Maximum sliding velocity $v$ (mm/s)	Maximum pressure $P$ (Gpa)
1	10	3
2	10	1.5
3	100	1.5
4	500	1.5

The 500 mm/s is not feasible due to centrifugal forces in the rotating cup, resulting in no seawater in the contact. Besides, at high speed, even during summer conditions the lubrication regime is most of the time in the mixed area (see Table 7). This means only cases 1 to 3 are experimented on. Case 2 is not a real case but is used to determine the influence of velocity, and could be present if one of the low-load applications does not run at full speed. A high-velocity high load case is not useful to experiment on, as this will not be designed and thus not be present in reality.

#### 5.1.5.1 Calculating loads

To achieve the same contact pressure as in a real system, the Herzian contact theorem of elliptical contacts is used. The force to meet the same pressure is shown in Table 14. The E-modulus of the base material is used on all materials. This way, a different E-modulus is beneficial as will also be the case in the real situation.

Table 15: Loads required to apply the required pressures

Load case	Pressure	Load
1	3	351.7
2	1.5	44

### 5.1.6 Sliding distance

Two pure sliding experimental phases can be distinguished: sliding distance with different intervals and the complete sliding distance, measured once at the end. The intervals are used as a pretest to know how wear will behave over time and if it is steady when the total sliding distance is reached, as is shown in Figure 2.12. This is due to its slow throughput time, only used on the first batch of samples. The final experiment is the 'false' wear, measured only once at the end. The pretest included a stationary disc, laser-cladded with Stellite 21 and E690 as a rotating disc. The slow throughput time was due to cleaning and measuring in between the sliding experiments, which all adds up to the experimental time. The volume loss is measured and the measured points are connected via interpolation. In Figure 5.5 and Figure 5.6 can be seen that the volume loss (and thus wear) stabilizes within the sliding distance of 60 m. The lubricating solution (NaCl) is slightly different from seawater and only one material combination has been experimented upon. Besides, due to production differences in shape and roughness are present however, this indicates that the sliding distance is enough for these experiments to show stable wear. It is assumed this is the case for other cases and the final experiments too.

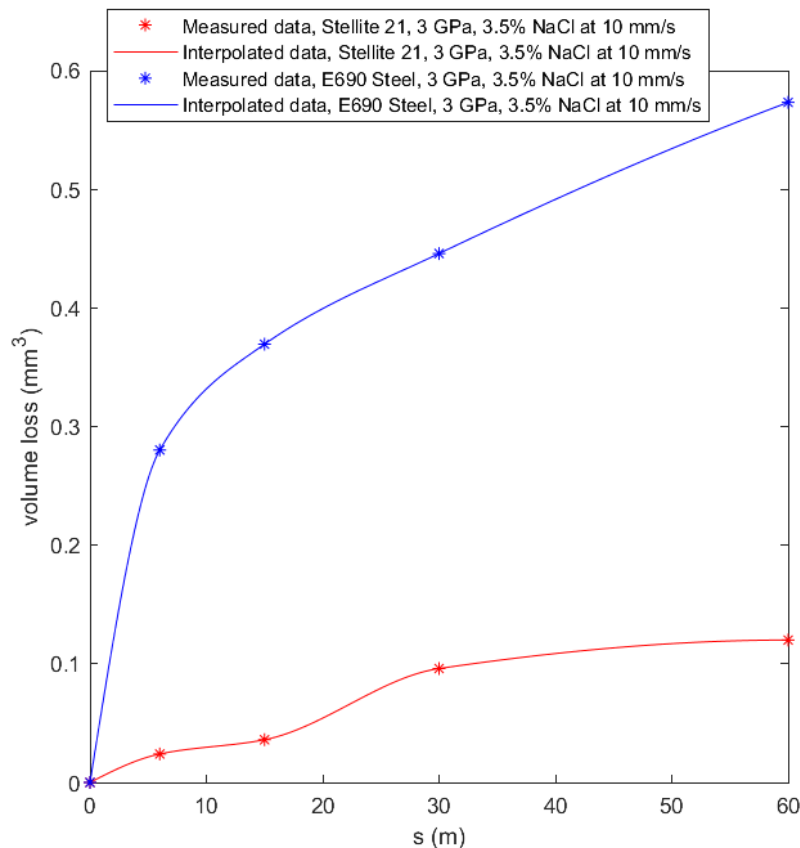


Figure 5.5: Volume loss of Stellite 21 and E690 in 3.5% NaCl solution lubrication for high load and low velocity. Interpolation is used to connect the measured points.

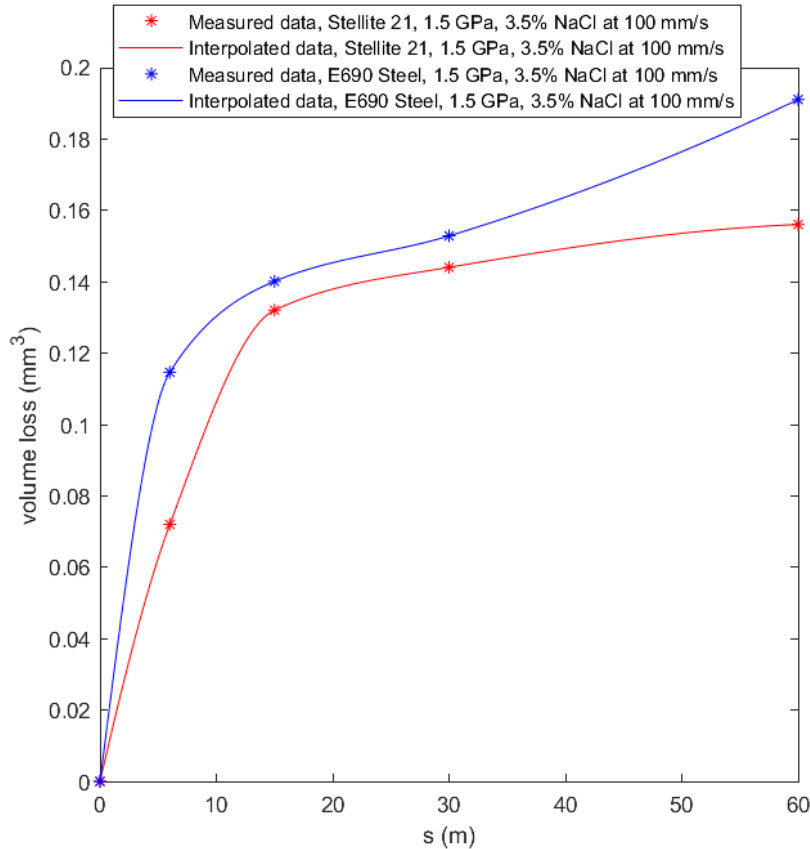


Figure 5.6: Volume loss of Stellite 21 and E690 in 3.5% NaCl solution lubrication for low load and high velocity. Interpolation is used to connect the measured points.

### 5.1.7 Experimental matrix

The experimental matrix is shown in Table 16.

Table 16: Experimental matrix

Case	Sliding velocity	Load (N)	Lubrication type	Sliding distance (m)
1	10	351.7	Seawater solution	60
2	10	44	All	60
3	100	44	Seawater solution	60

- To experiment with the influence of lubrication, lubrication is varied, with all other parameters constant. Case 2 is used for this. The grease-lubricated case is experimented on, only for the uncoated steel (18CrNiMo7-6).
- To experiment with the influence of load, the load is varied and thus cases 1 and 3 are compared.
- To experiment with the influence of the velocity, the velocity is varied and thus cases 2 and 3 are compared.
- To experiment with the influence of hardness, the hardness of the materials is varied and thus differences in the results for different materials in a case are compared.

All experiments are done for both rack materials and all pinion materials, except for the grease situation. For each influence experimented, one pinion material, randomly selected is a repetition.

## 5.2 Data measurement

Wear can be quantified by measuring the mass loss or the volume loss. The most advanced and precise weighing scale was found to be too much off with quantification as the mass loss was found to be in the error regime (0.1 mg [58]) for the stationary disc. For that reason, this is not used to measure wear. The samples are measured with the 3D optical profiler (Sensofar S Neox [59]) using the confocal microscope setting. A 3D height profile image of the surface is made from which volume loss can be extracted.

Friction is measured directly by the UMT.

To see the surface characteristics and morphology in more detail, the Keyence VHX 7000 Light Optical Microscope [60] is used with the required settings.

## 5.3 Data processing

### 5.3.1 Rotating disc

In Sensoview (the software that comes with the Sensofar profilometer), the Sensofar data is filtered: tilting is removed. Besides, spikes are removed and data is restored for data points with missing information by tracing with outliers removed. In Matlab, the data is trimmed as the sides of the measured area show noise.

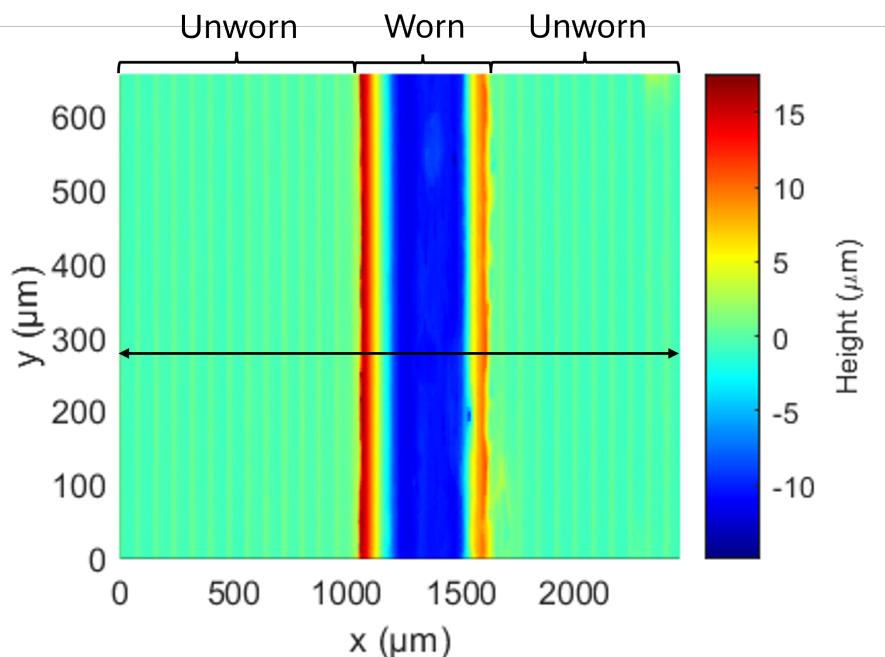


Figure 5.7: Wear track rotating disc, the worn and unworn areas are shown. The arrow indicates the direction of the slice.

The mean of the surface outside of the wear track is manually selected after plotting the data. The worn area is found by looking at the height profile. In Figure 5.7, the worn and unworn areas are indicated. The unworn area is a flat surface with only the roughness varying (greenish) with the worn area as a boundary. The worn area consists of wear and plastic deformation and thus peaks and valleys (red and blue). All data points are lowered by the mean value to be able to subtract the

wear data from the mean and thus do not influence the roughness. The whole wear track cannot be measured as it is too big and takes too much time, so only 1 rectangular spot is measured as shown in Figure 5.7. 100 lines are drawn through the wear track in the direction of the arrow. An example slice by a line can be seen in Figure 5.8.

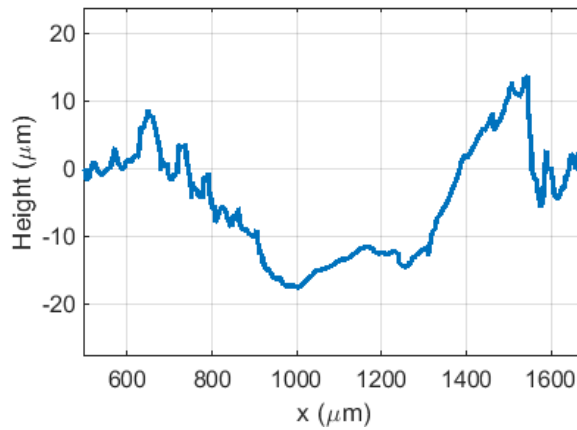


Figure 5.8: One slice. Equally distributed over  $y$ , 100 of these slices are made

For each line, it is evaluated what is below and above the mean. The wear area loss  $A_w$  is calculated by:

$$A_w = A_l - A_p \quad (41)$$

$A_p$  is the area that is displaced due to plastic deformation and is piled up.  $A_l$  is the area that is below the original surface and consists of wear and plastic deformation. This can graphically be seen in 5.9.

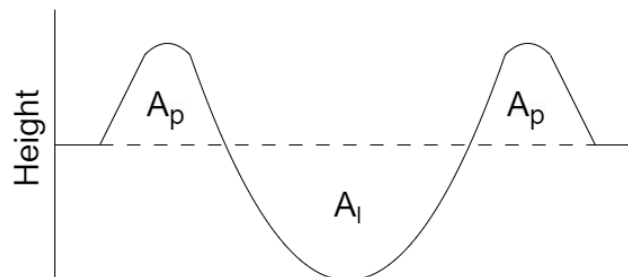


Figure 5.9: Schematic simplified representation of the slice with  $A_p$  the displaced area from plasticity and  $A_l$  the area lost underneath the original surface (dashed line)

Now the area loss is known. For each line, this is multiplied by the circumference  $C$  of the wear track, which is known.  $C = D * \pi$ . As 100 lines are measured, a box plot can be made to have statistical significance and because 100 lines are used, local defects can be ruled out.

### 5.3.2 Stationary disc

In sensoview, the pinion data is manipulated by removing spiking and restoring data points as described for the rack. This results in Figure 5.10 when imported in Matlab and trimmed as the sides of the measured area show noise.

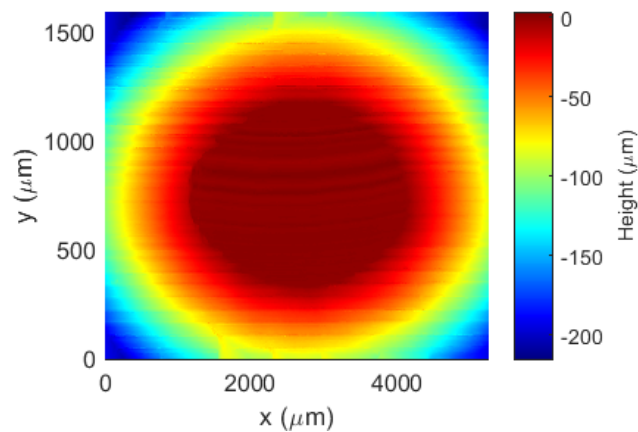


Figure 5.10: Data before form removal

To find the volume loss, it is important to be able to measure what is removed. It is chosen to remove the original shape of the surface. This is approximated by fitting a paraboloid, with a provided Matlab script [61] that uses a polyfit function in a least-square sense. In the input data for this paraboloid fitting, the worn area is marked and treated as Not A Number values. This results in a paraboloid as in Figure 5.11

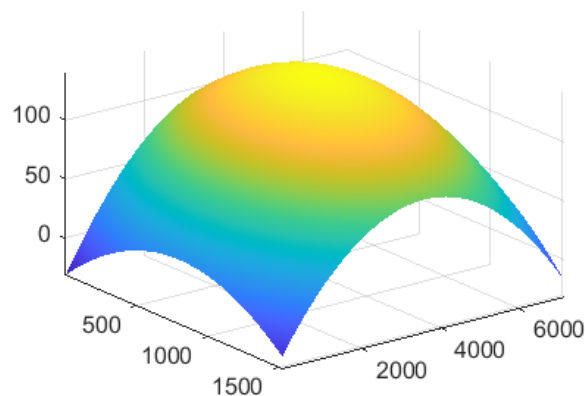


Figure 5.11: Paraboloid subtracted from the measured surface

This paraboloid is subtracted from the total dataset measured (Figure 5.10), and this results in Figure 5.12. The wear volume is the positive value of the total volume below 0 (the roughness is mean at 0). Again plasticity is covered by removing the positive values from this. This results in 1 value per experiment.

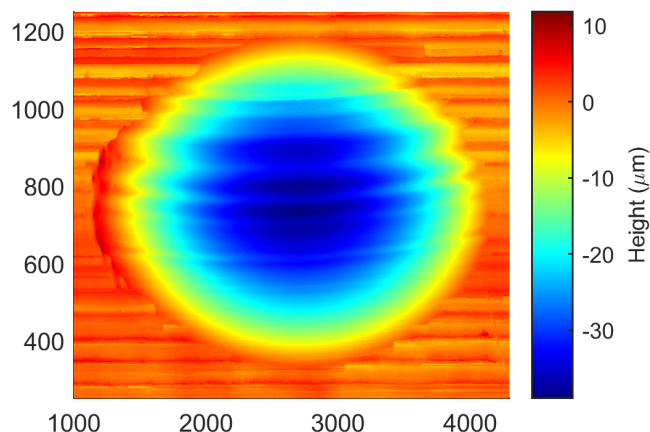


Figure 5.12: Data (wear) after form removal

The uncoated disc has a slightly different shape due to a different production. It is turned from both sides, instead of in one go as the rest is done. After measuring, this was found to be significant, so it was required to remove this shape.

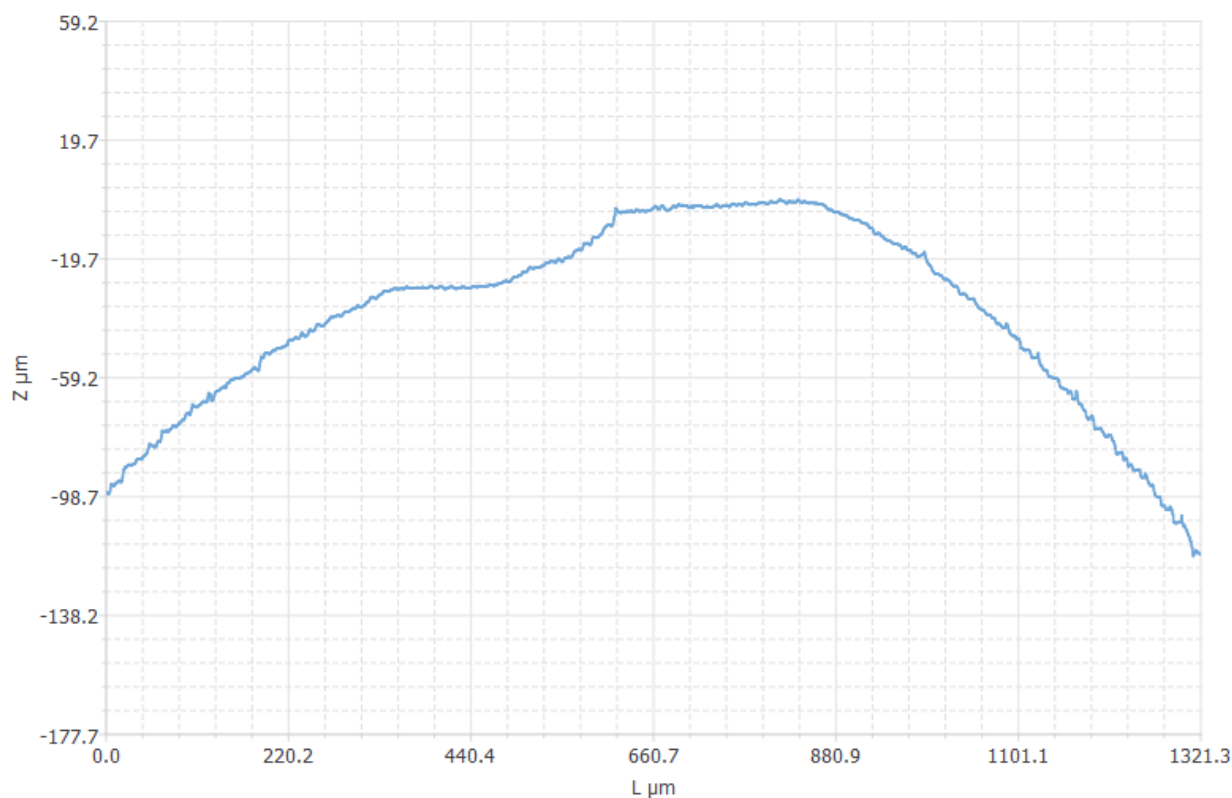


Figure 5.13: Uncoated disc with different shape on top

Therefore, the paraboloid is calculated for the uncoated disc by masking the whole width of this shape on top. After the paraboloid was removed, everything was flat except for the different shape. This is removed by taking the mean over  $x$  for all  $y$ . As a check, an unworn surface is flattened. In Figure 5.14 can be seen that the shape, is now almost completely flat and at least in a roughness regime.

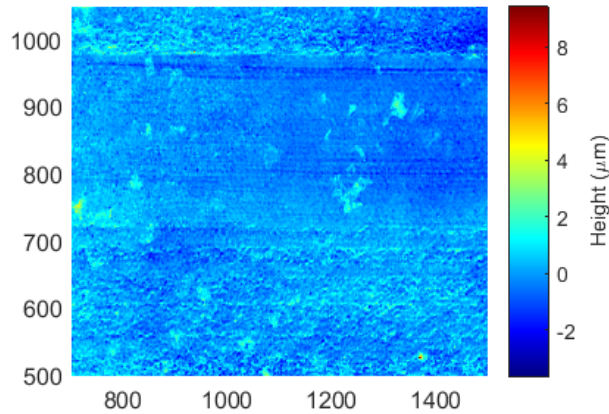


Figure 5.14: Uncoated disc flat

A wear profile of this uncoated disc is slightly different and not exactly elliptical (as the contact is not exactly elliptical) and looks like this:

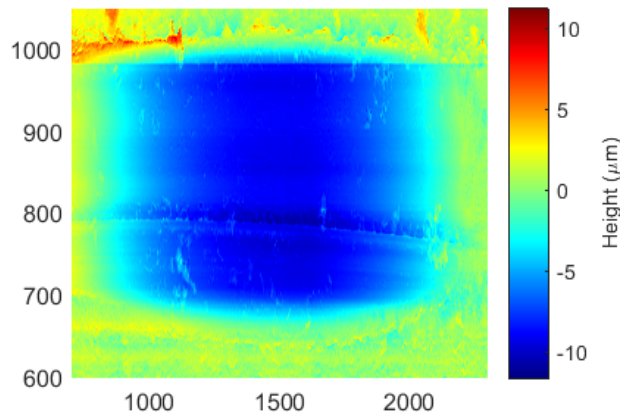


Figure 5.15: Uncoated disc wear profile

### 5.3.3 Roughness

Based on the previous analysis the roughness is calculated outside the wear track/area, with the flattened surfaces that have the mean of the roughness at 0. The average roughness  $S_a$  and root mean square roughness  $S_q$  are calculated as follows:

$$S_a = \frac{1}{MN} \sum_{i=1}^M \sum_{j=1}^N |z(x_i, y_j)| \quad (42)$$

$$S_q = \sqrt{\frac{1}{MN} \sum_{i=1}^M \sum_{j=1}^N (z(x_i, y_j))^2} \quad (43)$$

### 5.3.4 Coefficient of friction

The coefficient of friction is a direct output from the UMT. This is used as input for Matlab and plotted. It was found that high-frequency noise was present. This is only a problem for visualisation

and as the method depends on visual characterisation (for selecting a steady-state friction), a low-pass filter is applied to filter these high frequencies out. The sampling frequency of the UMT for the experiments was set at 100 Hz. After a Fourier plot is made, it was seen that frequencies below 0.05 are dominant, and all above that is treated as noise. This value is chosen as the cutoff frequency and as no exact amount of removal is required, no fast rolloff is required. Thus, a second-order lowpass filter is used with a cutoff frequency of 0.05. As a check, the original signal and filtered signal are compared. The filter has no influence on the mean as the characteristic of white noise is a mean of 0. The standard deviation is almost not influenced as the low frequencies are dominant.

After filtering the coefficient of friction shows a peak at the start resulting from static friction. In motion, the coefficient of friction stabilized and from the stable point onwards it is analysed as shown in Figure 5.16. The friction coefficient is presented as bar plots that present the steady-state friction with fluctuations and stability in this steady state presented by an error bar showing the standard deviation.

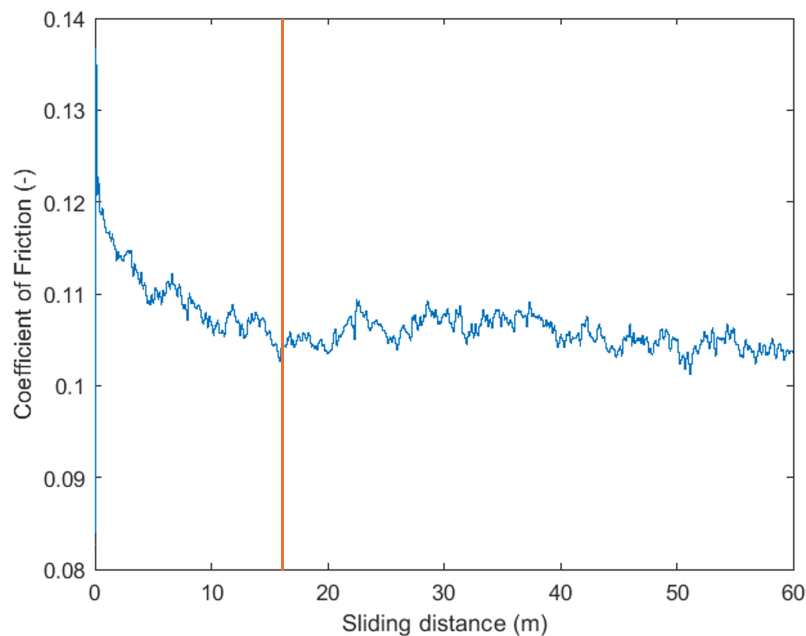


Figure 5.16: Coefficient of friction over sliding distance, the orange line indicates the starting point stable friction

## 6 Experimental results

The hardness and roughness results are shown in subsection 6.1 and Table 18. The wear and Coefficient of friction results are described in detail in subsection 6.3. Some results are found to be unreliable or were not possible to visualise which is discussed in subsection 7.4

### 6.1 Hardness measurements

The measured hardness of the material used in wear experiments is shown below:

Table 17: Hardness of the materials used in the experiments

	Rotating disc material		Stationary disc material			
<b>Material</b>	E690	42CrMo4	Uncoated	Stellite 21	Stellite 6	Stellite 190
<b>Hardness (HV)</b>	249	298	640	362	437	551

### 6.2 Roughness

The roughness of the used samples as measured is shown in Table 18

Table 18: Roughness measured on the samples used

	Roughness Sa	Roughness Sq
<b>E690</b>	0.53	0.60
<b>42CrMo4</b>	0.58	0.70
<b>Uncoated</b>	1.59	2.23
<b>Stellite 21</b>	1.29	1.54
<b>Stellite 6</b>	1.44	1.78
<b>Stellite 190</b>	1.21	1.51

### 6.3 Wear and Coefficient of Friction results

The wear of the rotating disc is a probability expressed by box plots evaluated over the 100 slices put through the wear track. The stationary discs are measured over the total wear spot. Some are measured as a repetition and those are presented with error bars that show the standard deviation. The coefficient of friction is presented as a bar graph with error bars that show the standard deviation of the steady-state part. The surface morphology of the rotating discs is displayed using height profiles, as the pictures from optical microscopy showed corrosion for some experiments due to the inability to measure directly. To compare, the conditions must be the same, which the case is with the height profile. The Pinion material wear morphology is shown by optical microscopy images as these materials are (mildly) corrosion resistant. When comparing the different influences, all other parameters are kept the same.

#### 6.3.1 The influence of different types of lubrication

The wear rates of E690 with different counter materials are presented first. This is then followed by the wear rates of these (stellite) counter materials. The friction coefficient is then shown. At last, the wear morphologies are shown.

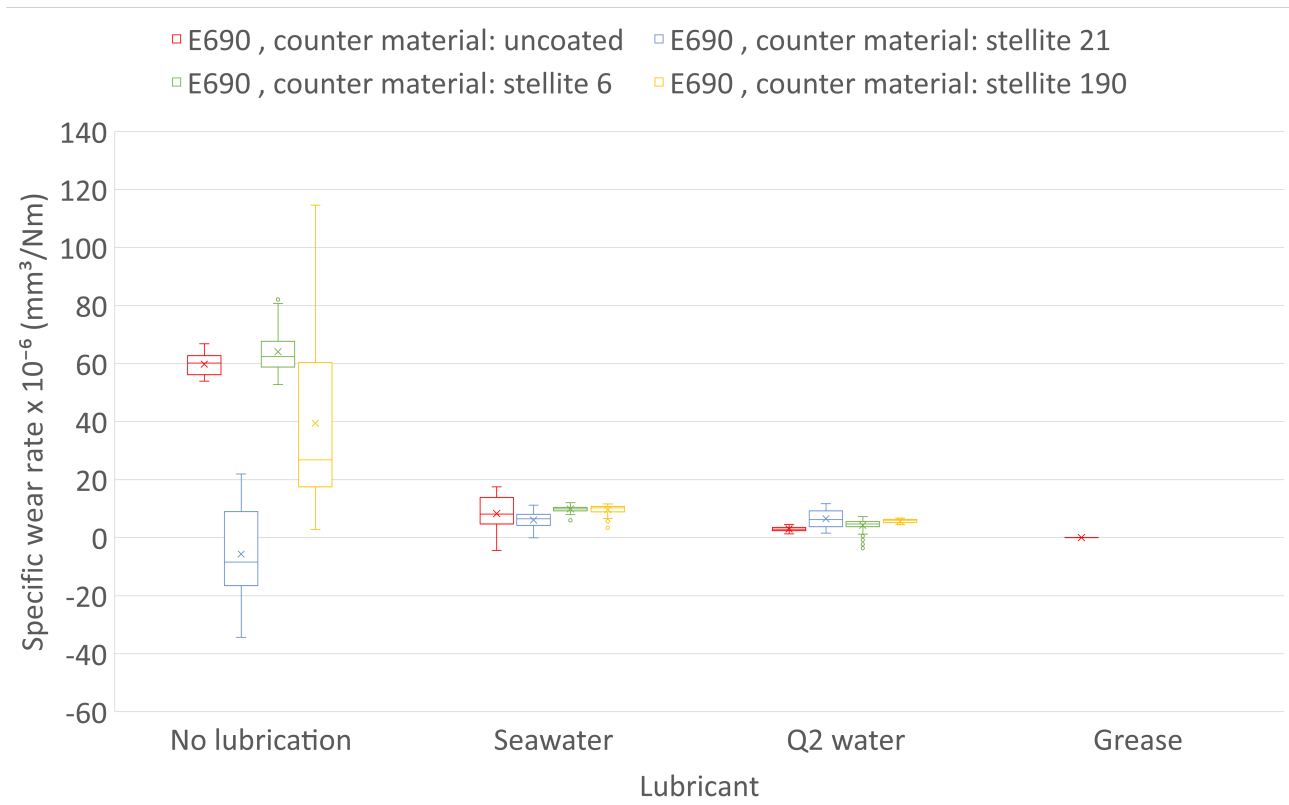


Figure 6.1: Wear rates of the E690 with different stationary discs as a counter material and different types of lubrication

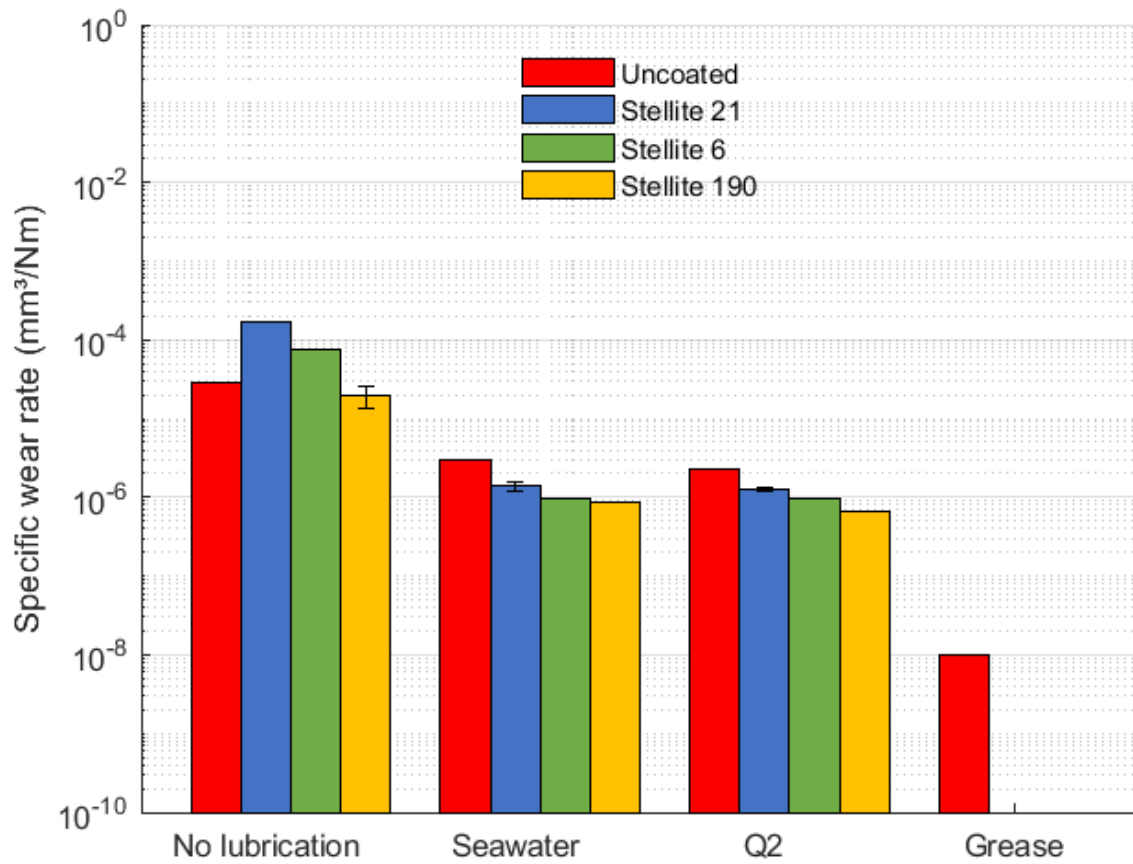


Figure 6.2: Wear rates of stationary discs with E690 as counter material and different types of lubrication. A logarithmic scale is used

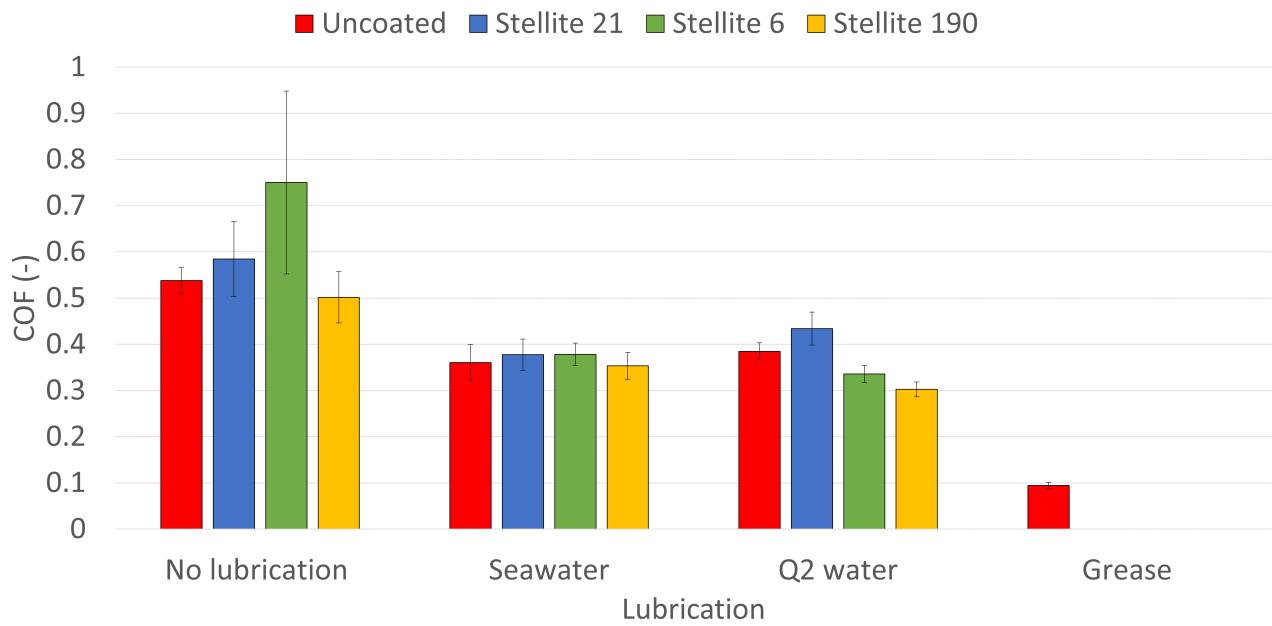


Figure 6.3: Coefficient of friction of stationary discs with E690 as counter material and different types of lubrication.

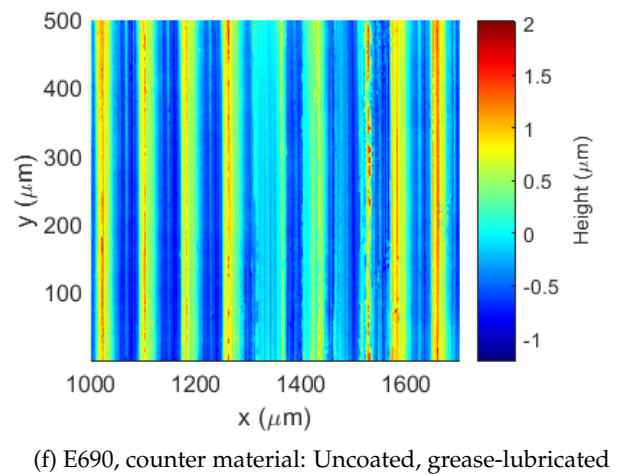
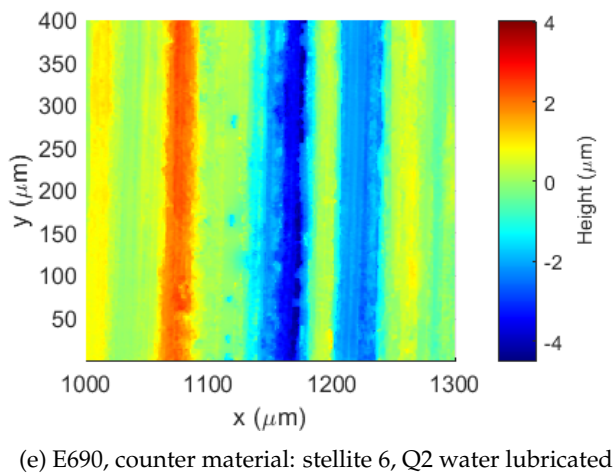
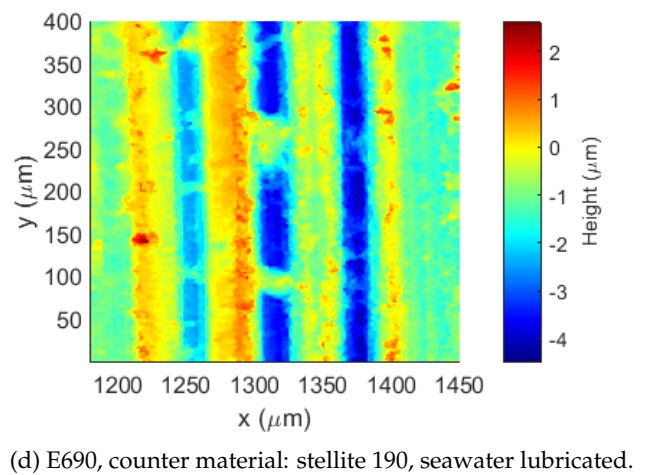
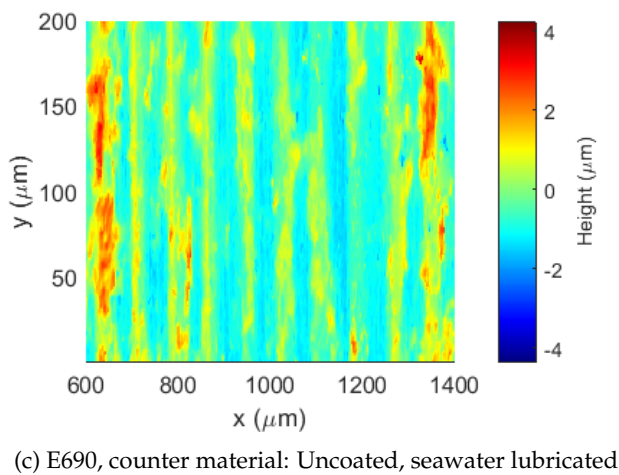
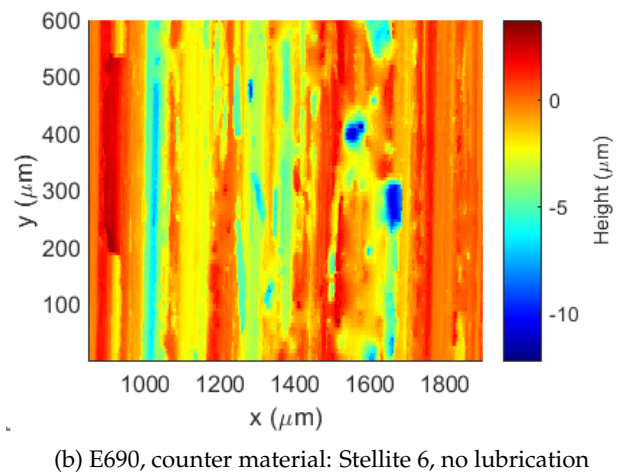
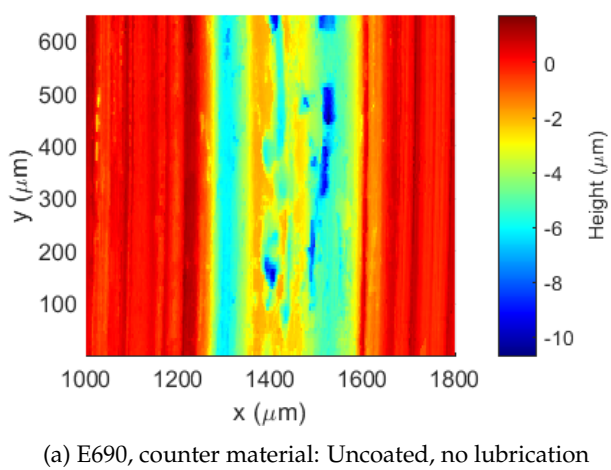
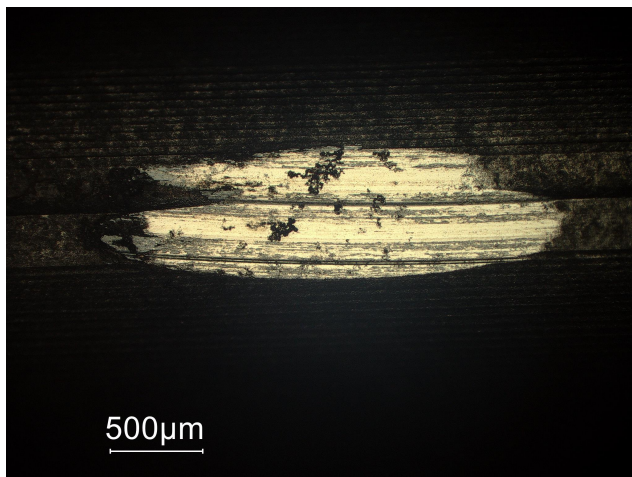
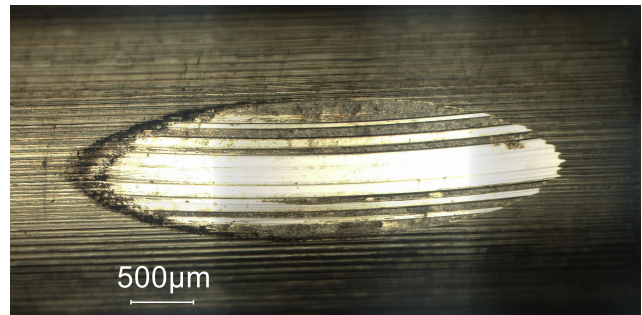


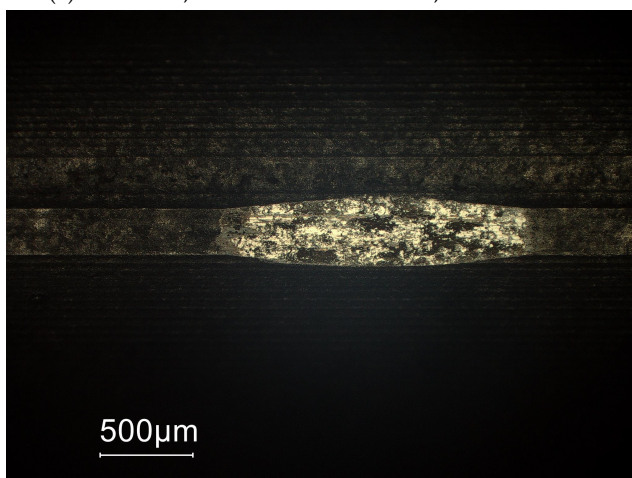
Figure 6.4: Wear morphologies rotating disc



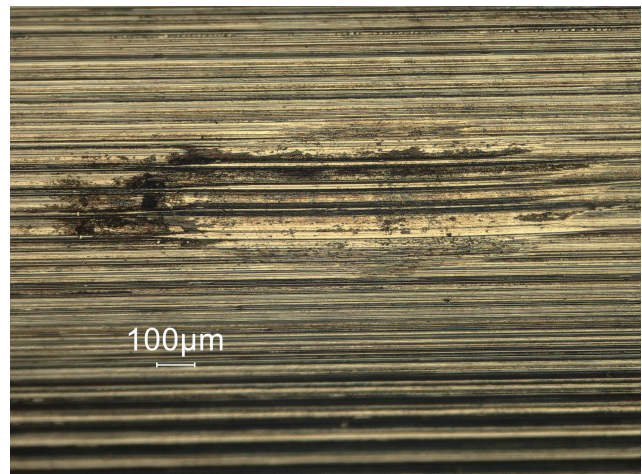
(a) Uncoated, counter material: E690, no lubrication



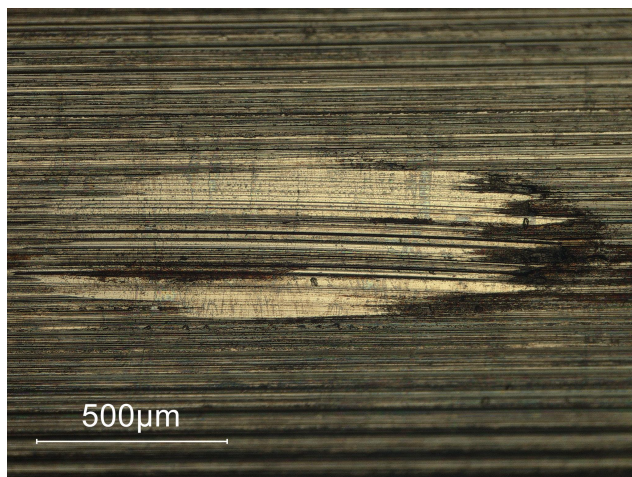
(b) Stellite 6, counter material: 42CrMo4, no lubrication



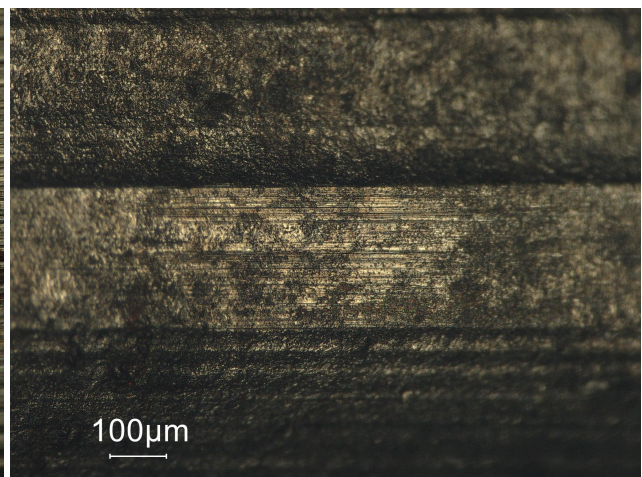
(c) Uncoated, counter material: 42CrMo4, seawater lubrication



(d) Stellite 190, counter material: E690, seawater lubricated



(e) Stellite 6, counter material: E690, Q2 water lubricated



(f) Uncoated, counter material: E690, grease-lubricated

Figure 6.5: Wear morphologies stationary disc

It can be seen that different types of lubrication influence the wear and coefficient of friction. The wear of unlubricated sliding is the highest for the rotating and the stationary parts. The coefficient

of friction is also very high and unstable for the dry cases. All show cavities formed on the rotating discs in Figure 6.4, combined with some scratches. These cavities can be seen on a smaller scale on the stationary discs too, however, the scratches are the main morphology that can be seen in Figure 6.5a and Figure 6.5c.

Seawater and Q2 water show similar wear scratches in Figure 6.4 and Figure 6.5. Both have lower wear than dry wear on all stationary materials and have minimal difference from each other compared to dry and grease lubrication. On the rotating discs, the same holds, with in some cases a bit of overlap. The coefficient of friction is very similar with overlap for Q2 and seawater lubrication. No difference seems to be present in the wear type of the rotating disc, with different (cladded) counter materials as is shown in Figure 6.4a and Figure 6.4b. This is checked another time in Figure 6.4c and Figure 6.4d So for Q2 not all materials are shown. The corresponding pinions show the same.

The wear of grease-lubricated sliding could not be measured on the uncoated stationary disc because it was in the roughness range. However, for visualizing a very small value in the boundary lubrication regime is shown in Figure 6.2. The wear of grease lubrication is the lowest. The wear on the pinion could not be observed, so that is different from the other lubricants, where low wear on one material meant high wear on the counter material. Grease lubrication has the lowest coefficient of friction of all lubrication types experimented on.

Generally, it can be seen that the difference between Q2 water and seawater is very minor, and the difference between non-, (sea)water-, and grease lubrication is very big in terms of wear type and rate.

The same trends as for E690 can be seen on 42CrMo4 and are shown in subsection 7.1.

### **6.3.2 The influence of load**

The same order as the influence of lubrication is followed.

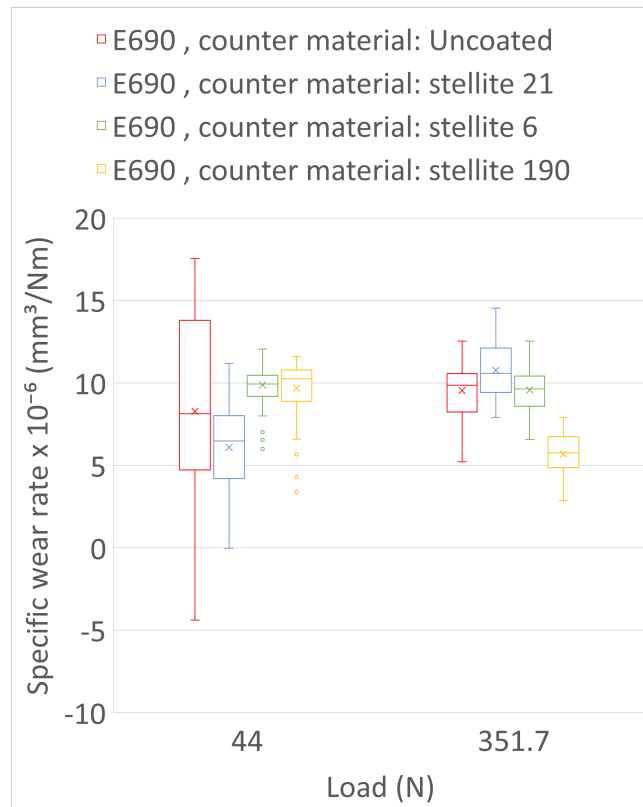


Figure 6.6: Wear rates of E690 with the different stationary discs as a counter material and varying load in seawater lubrication

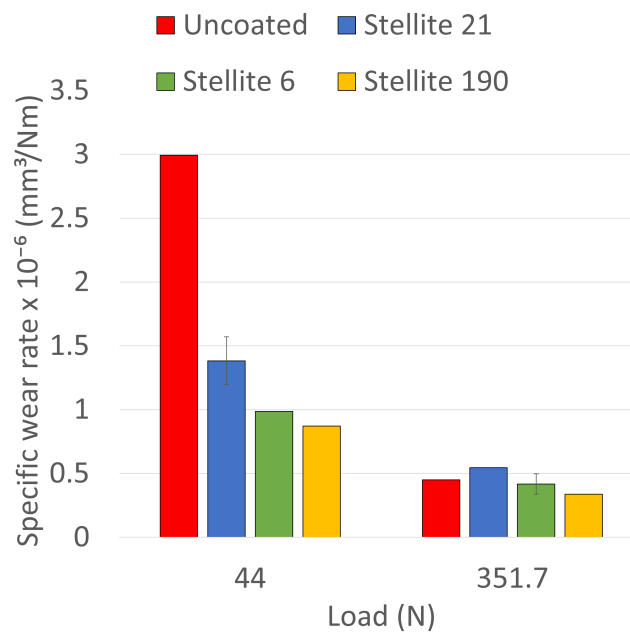


Figure 6.7: Wear rates of stationary discs with E690 as counter material and varying load in seawater lubrication

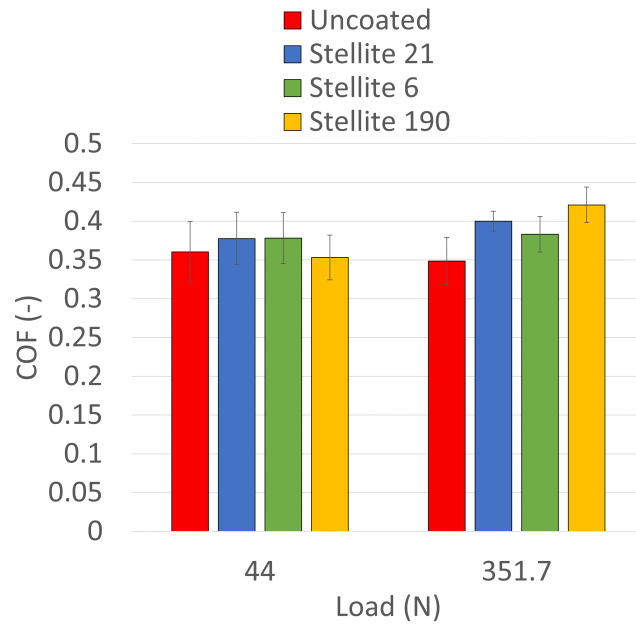


Figure 6.8: Friction coefficient of stationary discs with E690 as counter material and varying load in seawater lubrication

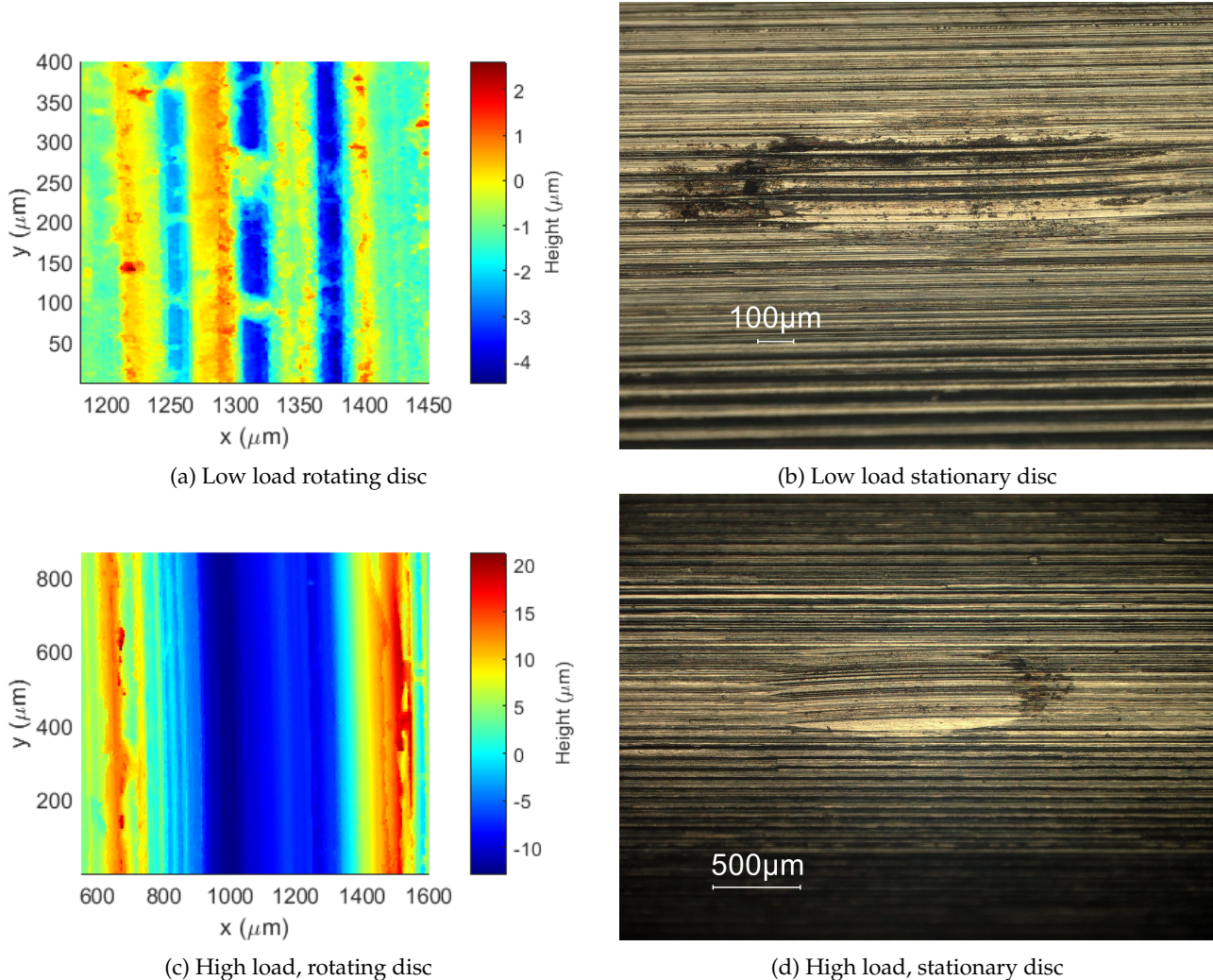


Figure 6.9: Wear morphology, load dependency

Only the cases with E690 can be compared for the varying load cases. It can be seen that against the base material, it has less spread in wear rate values for a higher load. This means a more stable wear rate over the circumference of the wear track. The stellites show very much overlap and no big distinguishment on the wear of the rotating disc. For the stationary discs, it is found that a higher load results in less specific wear with all materials showing similar wear. The coefficient of friction does not show a distinction for a high load as an overlap between the standard deviations is present. This holds between the different stationary discs as well as compared with the low load. The wear type in Figure 6.9c shows similar scratches as in Figure 6.9a, however, on a bigger width.

### 6.3.3 The influence of velocity

Again the same order is followed.

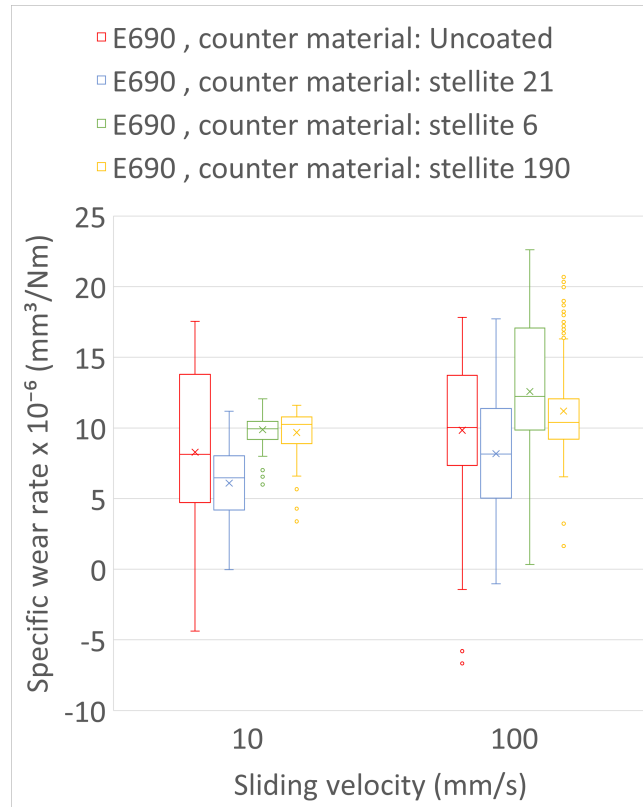


Figure 6.10: Wear rates of the E690 with different stationary discs as a counter material and varying velocity in seawater lubrication

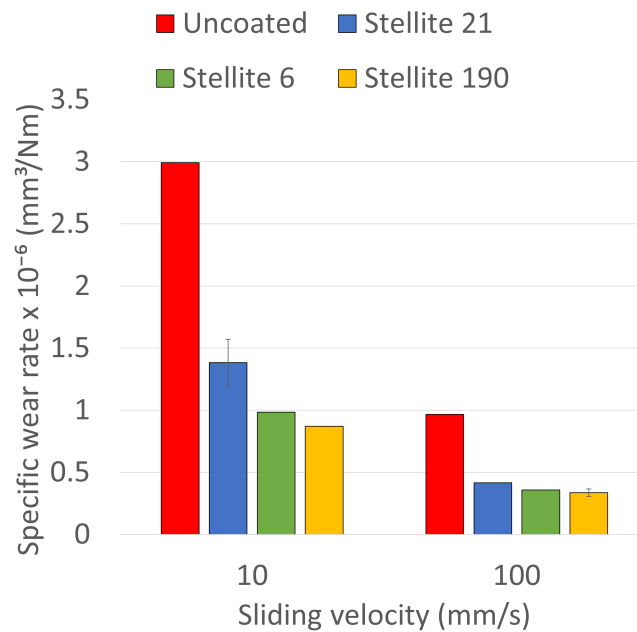


Figure 6.11: Wear rates of stationary discs with E690 as counter material and varying load in seawater lubrication

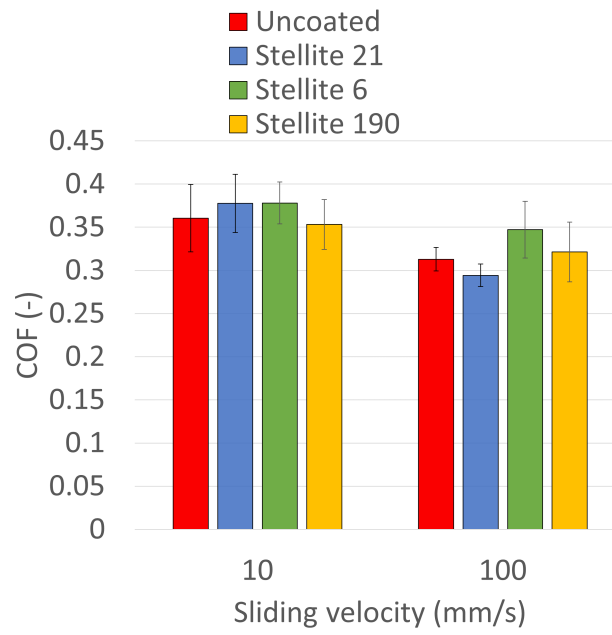
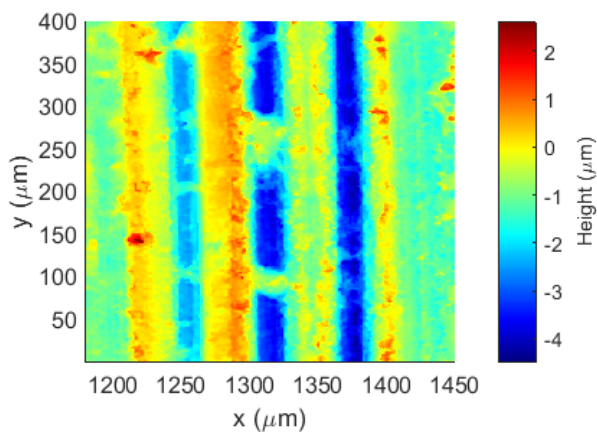
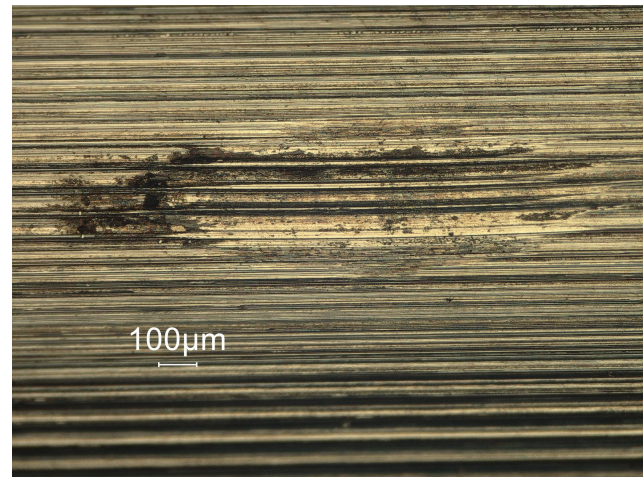


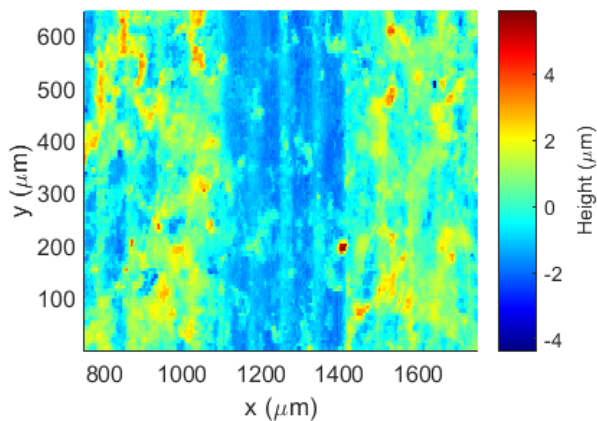
Figure 6.12: Coefficient of friction of the wear experiments of the stationary discs with E690 as counter material and different velocities in seawater lubrication



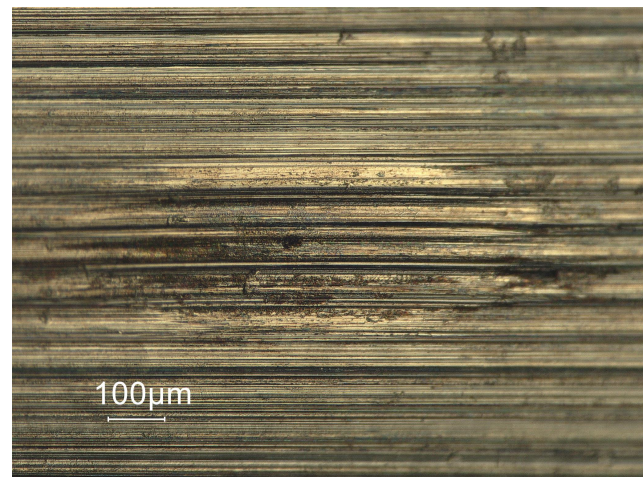
(a) Lowvelocity, rotating disc



(b) Low velocity, stationary disc



(c) High velocity, rotating disc



(d) High velocity, stationary disc

Figure 6.13: Wear morphology velocity dependence

A high velocity with seawater lubrication results in lower wear for all the stationary discs. Only the E690 experiments can be compared for velocity dependence. For E690, here generally more spreading is experienced for the stellites, meaning less stability. However, generally, it is very similar. Versus uncoated, the stationary disc is not changed much in terms of value and spreading. The scratches on the surface are similar as can be seen above. The coefficient of friction is lower in means with a higher velocity, however, a lot of overlap can be seen so it is very similar.

#### 6.3.4 The influence of the hardness of the rack and pinion material

Again the same order is followed.

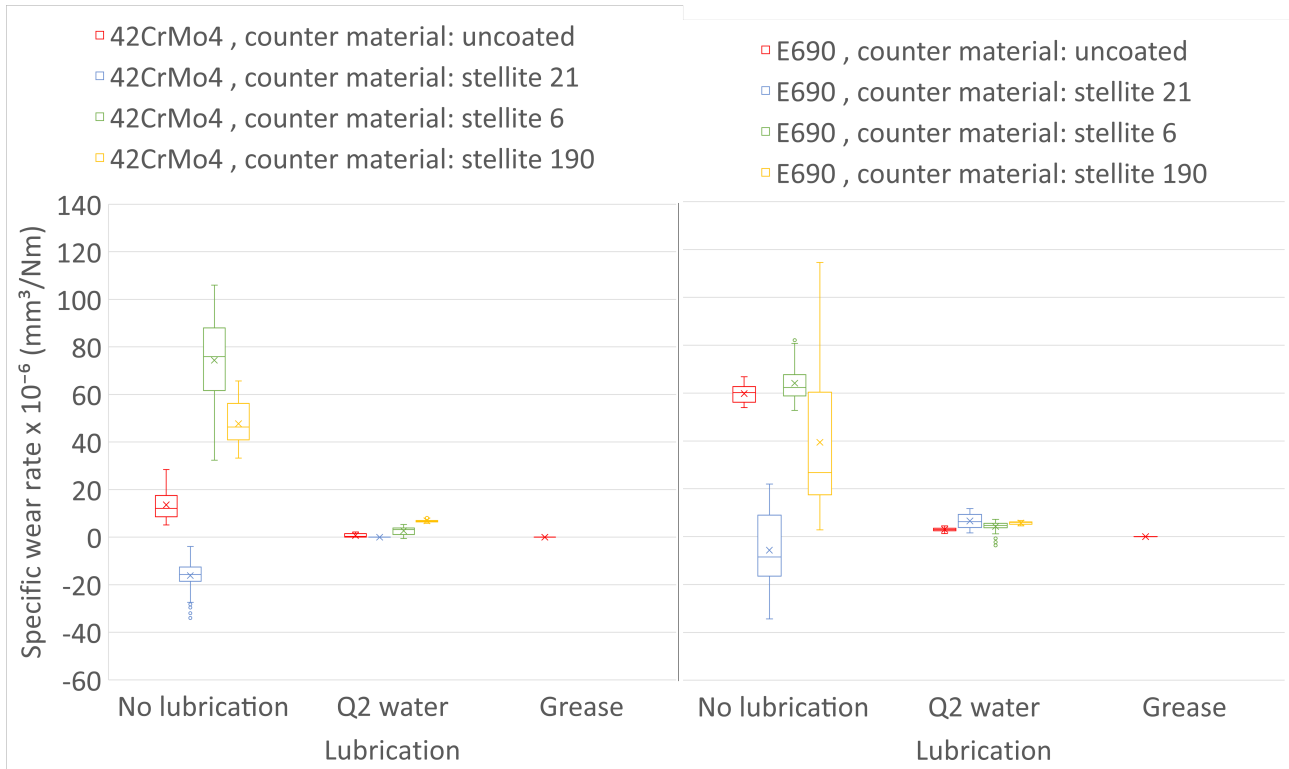


Figure 6.14: Influence of different rack material on wear of the rack. Rack materials are divided by the vertical line and are displayed on top of the subgraph

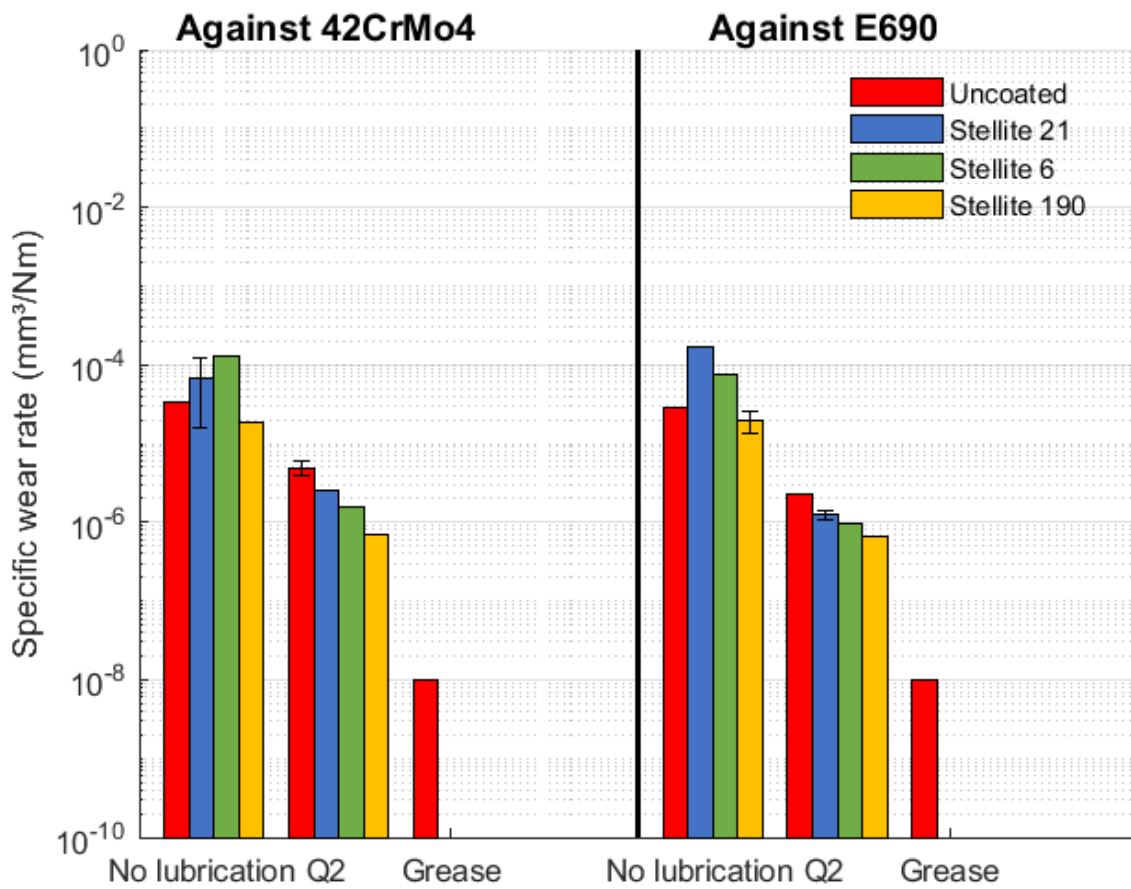


Figure 6.15: Influence of different rack materials on wear of the pinion. Rack materials are divided by the vertical line and are displayed on top of the subgraph

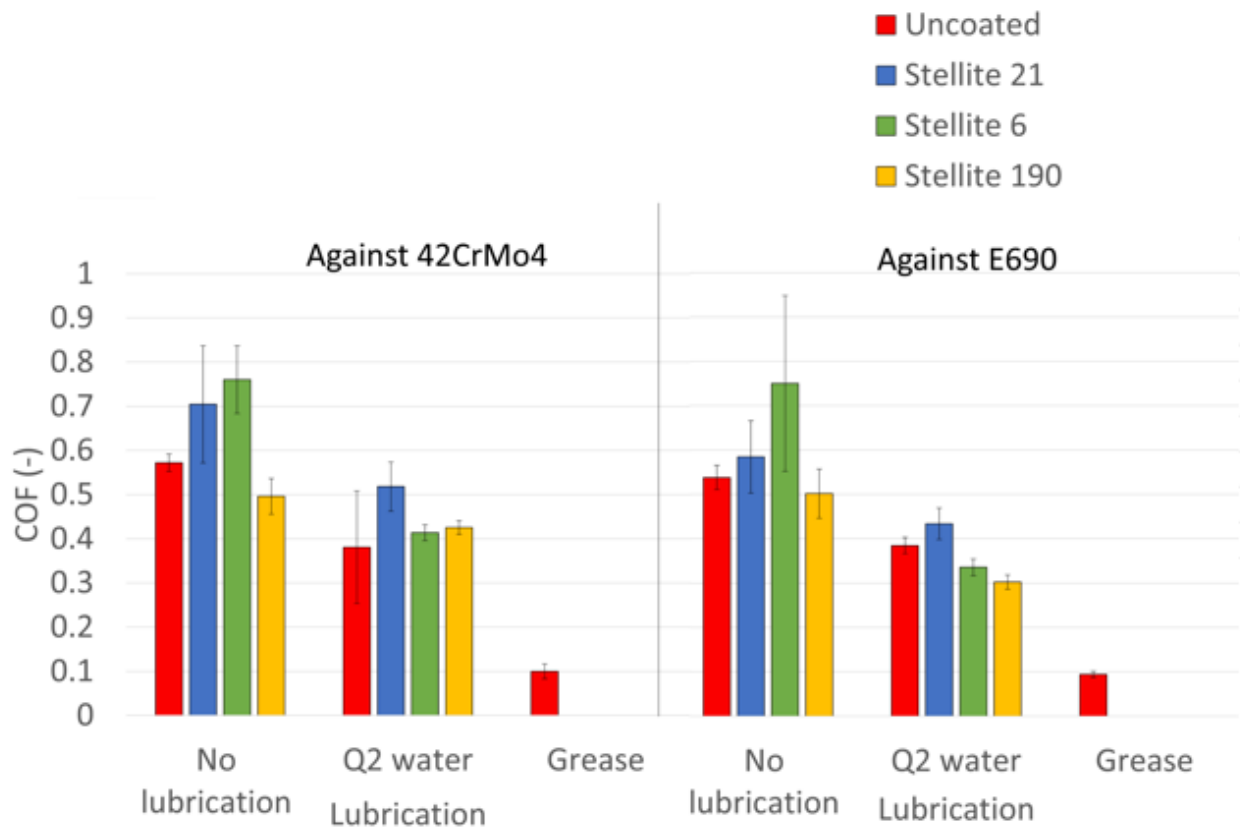
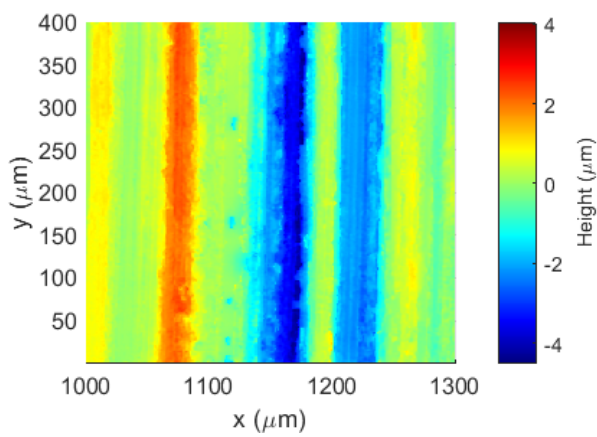
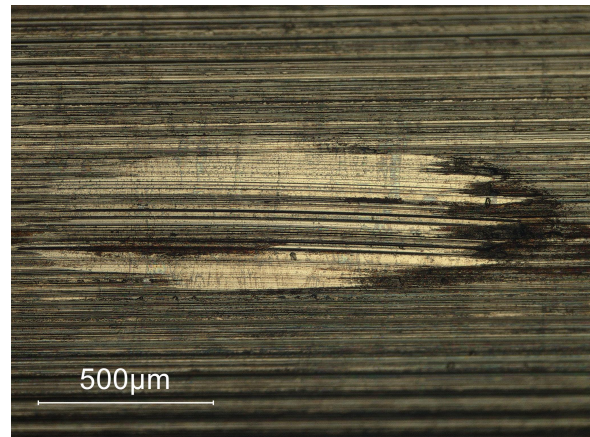


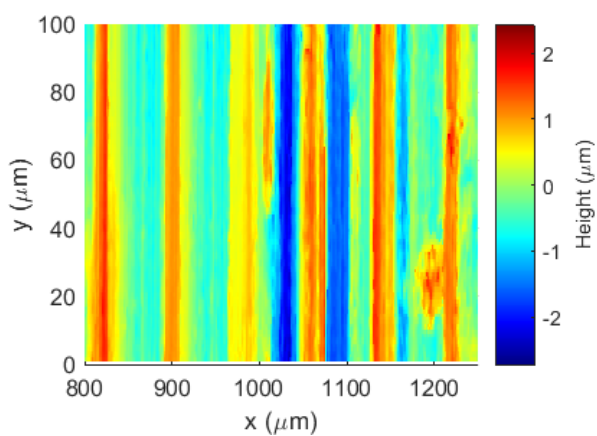
Figure 6.16: Influence of different rack materials on the coefficient of friction. Rack materials are divided by the vertical line and are displayed on top of the subgraph



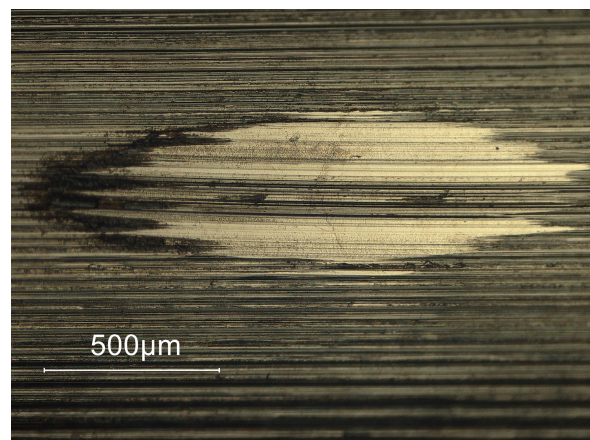
(a) Q2 lubricated E690, counter material: stellite 6



(b) Q2 lubricated stellite 6, counter material: E690



(c) Q2 lubricated 42CrMo4, counter material: stellite 6



(d) Q2 lubricated Stellite 6, counter material: 42CrMo4

Figure 6.17: Wear morphology hardness influence of the rotating disc

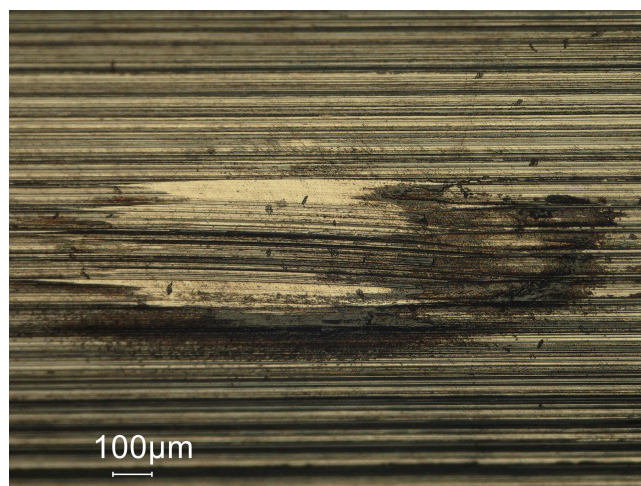


Figure 6.18: Wear morphology Q2 lubricated Stellite 190, counter material: 42CrMo4

The influence of the hardness of the rotating disc on the wear of itself is not possible to determine as the difference is very low (factor 1.2). The influence of the hardness of the rotating disc on the

stationary discs, the same holds. When comparing the materials in Figure 6.14, a difference in wear is not present. For the coatings, an increase in hardness leads to a decrease in the specific wear rate on itself as can be seen when comparing the results in Figure 6.15. The uncoated material wear is higher or comparable with Stellite 21 for any of the lubricated situations. In the dry case, this is higher than stellite 190 but lower than the other stellites. The influence of the hardness of the stationary disc on the rotating disc is not visible. A lot of overlap in the box plots is present indicating the probability is very similar with some exceptions. For the non-lubricated case, it can be seen that stellite 21 has the lowest wear on the rotating disc. Furthermore, generally, the spread of stellite 190 on the rotating disc in lubricated situations is the lowest. This indicates the best evenness of wear in lubricated situations for stellite 190, the hardest stellite experimented on. The influence of hardness on the coefficient of friction is very minor as can be seen in Figure 6.3 and Figure 6.16. A lot of overlap is present. The only trend present is for Q2 water lubrication a higher coefficient for the higher hardness of the rotating disc, in contact with the stellite coatings. In contact with the uncoated steel, an overlap of the standard deviations is present.

## 7 Discussion

### 7.1 Hardness

The hardness found in Table 17 is for most materials as expected. The stellite coatings are all in the range of possible hardness [42] [44] [46]. The uncoated steel is case hardened and a bit lower than the value presented by the manufacturer (58 HRC = 746 HV), but close. The soft rotating disc (E690) was expected to be 25.6 HRC  $\approx$  257 HV which is very close to the measured value (249). The hardness of the quenched hard rotating disc (42CrMo4) depends on the temperatures and time of the quenching and tempering used [62]. In optimal conditions a hardness of 56 HRC = 694 HV can be reached. The measured value is much lower (298). The reason for this could be a wrongly used quenching process. This reduction in hardness is negative for this experiment as the hardness difference of the rotating discs is only factor 1.2. This means the hardness influence cannot be measured, as other effects can be more dominant than this small difference. In the calculations for the maximum contact pressure, no hardness effects are taken into account. The hardness of the softest material, however, is a limiting factor for the contact pressure. A lower hardness means more plastic deformation and thus a lower real contact pressure. This means the maximum contact pressure will not be reached. Originally a difference would be present with the hard material having a higher real contact pressure. However, now this difference will not be present.

### 7.2 Wear analysis

Based on the data (wear rate and microscopy images), the grease-lubricated situation is in boundary lubrication as the wear is in the roughness regime. This is true for the hard and soft rotating disc and was expected, based on the real-life situations and calculated in subsection 2.3. The grease showed to have a big impact (it reduced wear and friction coefficient) even with little and no continuous feeding. Just a small layer of oil was enough to reduce it throughout the experiment (see Figure 7.1). The friction stays stable during the stabilised situation and shows no increase in value.

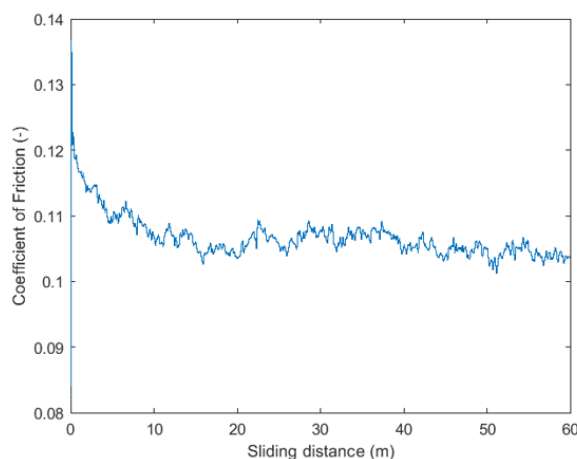


Figure 7.1: Coefficient of friction over time for grease-lubricated situation

Q2 water lubrication shows scratches (see 6.17 on the surface meaning abrasive wear. The wear rate of the softest material (the rotating disc) is lower than the range of unlubricated abrasive wear. The abrasiveness is very low. Oxidative wear should be present but has a low contribution as Q2 water is pure and contains no salts. Besides, the oxidative layer will be sheared off continuously. Seawater lubrication shows a similar scratch type of wear. This means abrasion is present in this lu-

brication type. Seawater increases corrosion very rapidly as it contains salts which increase general corrosion and tribo corrosion [63]. So corrosive wear does play a role in seawater however, it cannot be seen as a very thin layer is formed in the time of one rotation. This layer is sheared off and formed continuously as discussed in subsection 6.3

Figure 6.4a and Figure 6.4b show small pieces of material removed from the surface indicating adhesive wear that happened in dry sliding [64]. This is true for stellite 6, based on literature [65]. This would be due to galling (similar to cold welding)[66]. The coefficient of friction being high and unstable (high standard deviation) supports this. Adhesive wear can have a wide range of specific wear rates but in this case, it is more severe than the observed abrasion. This wear is also very unstable as can be seen on the coefficient of friction as it has a very big standard deviation.

In [67], it is discovered that wear rates of wear resistance steels with a ceramic ball indenting show wear rates in descending order: dry, seawater and distilled water. [45] shows that for steel and stellite 6, water decreases the wear rate compared to dry sliding as well. This seems to be true for all stationary materials (coatings and uncoated). Q2 water and seawater are very similar. The wear of both seawater and Q2 water lubrication is abrasive and oxidative (as oxides are formed in a water environment). The lowest wear (on both rotating and stationary discs) can be observed in grease lubrication. This is because boundary lubrication is present and was expected based on subsection 2.3. All stellites perform better than the uncoated steel except for the dry and greased contacts. This difference is, however, lower than the difference between the types of lubrication. Besides, in a real situation, the pinion makes more cycles than the rack, so it is allowed to have higher wear on the rotating disc as long as the stationary disc performs well.

It is generally known that the hardness of the softest material contributes to abrasive wear [3] however, as many other parameters determine the wear coefficient it cannot be stated that a higher hardness directly increases wear resistance. An increasing hardness, results in a lower wear rate for these experiments within the stellite coatings. The uncoated material has a higher wear rate for (sea) water-lubricated contacts while having the highest hardness. This can be related to the composition of the metals as can be found in 13. Stellites are cobalt-based alloys that are known for their high wear resistance [6][68][69][70]. So with the same base material, hardness does influence the wear rate. With another base material, hardness does not influence the wear rate, but the wear rate behaves differently. The hardness is changed by different elements that are added to the structure. With carbides, hardness is increased for stellites [71][72]. Stellite 190 has a higher carbide concentration than stellite 6 and stellite 21 (this is proportional with C atoms that are present to form carbides). An increased amount of carbides leads to a reduction in wear [71] [46]. So hardness indirectly influences the wear of the stationary discs for the same base material but the carbides do directly for all materials in this experiment as the lowest wear is present in stellite 190 followed by stellite 6 and stellite 21. Normally the coefficient of friction of steel is expected to be the highest for steel-steel, be it very minor [45]. For dry wear, this is the only case where this is not true. A possible reason is that hardness plays a big role in the wear and coefficient of friction of the dry contact and not the composition as the uncoated material is hardened and for that reason is known to have good tribological properties [56].

No big influence of the hardness of the stationary discs on wear can be found on the rotating discs. Much overlap is present. All coatings (and uncoated) are harder than the rotating discs so they will abrade the rotating disc. Both hardness are about the same so not much can be said about that.

In the hard rotating disc, a higher carbon content should give a higher resistance to wear [73]. The Carbon content increases the hardness and the wear resistance. However, this is only visible for the Q2 water-lubricated situations and non-lubricated wear, with an uncoated stationary disc. All other

cases show overlap and no distinguishment can be made on that. The carbon content and hardness are very close to the soft rotating disc, which could be the reason for no visible difference. many other things could have been present if a difference had been measured.

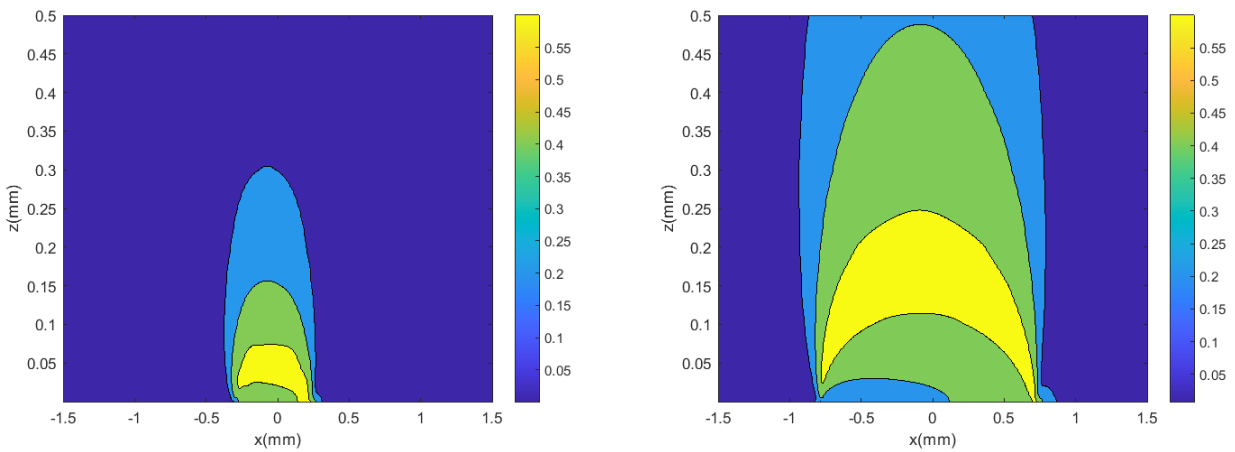
It is found that for the experimented cases, a higher load leads to a lower specific wear rate (abrasive and/or corrosive). Load influence is very case specific as found in literature. For cobalt-chromium alloys, it was found that a higher load reduced the specific wear rate in a specific case [74]. The same is generally found for steels [75][76]. A simple explanation is an increase in the contact area. With a higher load, more plastic deformation will be present. This increases the contact area and results in a non-proportional wear increase compared to the load increase. The much higher width of the wear track can be seen in Figure 6.9). The total worn volume is higher but as the specific wear rate is normalized over the normal load, this results in a lower value. This corresponds with the Archard wear law:  $V = k \cdot F \cdot s$ . If a slightly higher volume but much higher force, specific wear will be lower.

A higher velocity leads to less wear on the stationary pin and a lower coefficient of friction. The results can vary a lot per material, but generally, indeed, a higher velocity increases wear [77]. When oxidation takes place, lower values can be found. All stellites form oxide layers due to their high chromium content and Cobalt content [78] [22] [79]. The content can be seen in Table 13. These oxidation layers are strong and dense and are known to prevent them from corrosion. As the uncoated steel has the same drop as the stellites as can be seen in Figure 6.11, it is assumed that this layer is also formed on the uncoated steel. Severe wear is not present, so it is assumed that abrasive oxides were not the main oxides present. Increasing the velocity increases the temperature at the contact spots. This increases the formation of oxides that protect the surface and result in a lower wear rate [80]. This oxide layer is very thin and is difficult to observe with microscopy. Another possible reason could be an increase in plastic deformation, however, this does not seem to be true as no deformation can be seen. A fluid film will not be achieved with seawater so this could not be the reason for lower wear in higher velocity. So the only possible reason is the formation of an oxide layer.

### 7.3 Onset of plasticity at the surface

The onset of plasticity can be calculated and is generally known for a Herzian line- and point contact. This indicates at which coefficient of friction subsurface cracks no longer initiate subsurface but at the surface. For both line and point contact, this is understood to be a friction coefficient of 0.3 [3] [81], where Hamilton equations can be used for a point contact [82], while a line contact requires numerical integration.

To prove plasticity in the experimented situations, simulation is done based on the code that was provided and elaborated in the following paper: [83]. This results in the following values: a friction coefficient of 0.15 for a high load and a friction coefficient of 0.25 for a low load. The difference in E-moduli and hardness (only of the soft material as this is the limiting hardness) does not change much in the values, so the different materials have no influence. The result is that plasticity on the surface is present at all times and cracks will no longer be parallel to the surface but transverse to it [3].



(a) Low load simulation at a coefficient of friction of 0.25      (b) High load simulation at a coefficient of friction of 0.15

Figure 7.2

#### 7.4 Invalid results

Some results were found to be invalid or unusable. This was mainly due to corrosion.



(a) Seawater

(b) Q2

Figure 7.3: Corrosion on rotating discs

No wear rates could be determined on 42CrMo4 with seawater, as severe corrosion was present on the material as can be seen above. As the discs were not stored in oil, general corrosion happened as can be seen in Figure 7.3a. For the (sea)water lubricated situation, no microscopy figures are present as it corroded mildly so this would not give reliable images as can be seen in Figure 7.3b. For this reason, only the height profiles are used to characterise the wear morphology of the rotating discs to be able to be compared.

## 7.5 Validity of the results used in this research

In this section is discussed to what extent the results used in this research are valid.

### 7.5.1 Number of measured spots

During data measurement, it was decided only to measure the rotating disc at one rectangular spot. One could argue multiple spots are required to take tilting into account. However, maximum flatness and parallelism were set for production as can be seen in Figure 5.3d. These requirements are checked afterwards and are met. Besides, the leaf spring assembly is mounted to keep the normal force constant and account for roughness and the small tilting that still can be present. One wear measurement at 4 different positions north, east, south and west is done. In Figure 7.4 can be seen that the resulting values show overlap, meaning only small differences between the spots are present which are allowed to be neglected. This means measuring at 1 spot is viable.

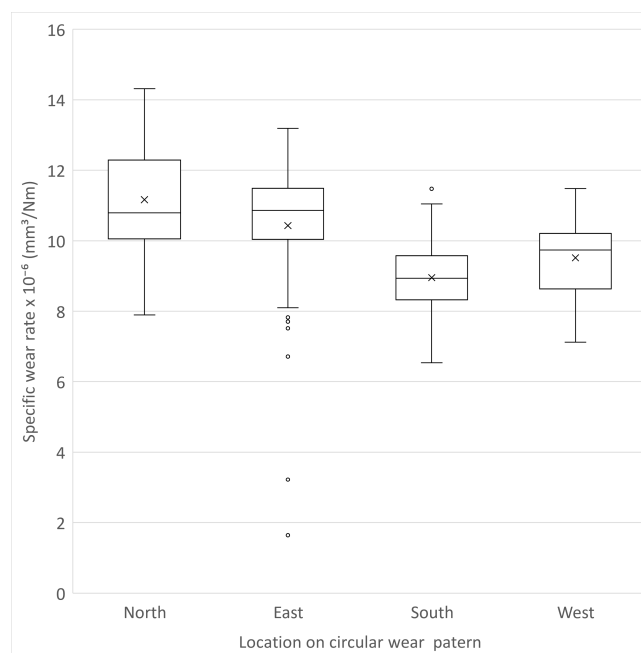


Figure 7.4: Position dependence of the wear position measured

### 7.5.2 Influence of plasticity on measured wear

Plastic deformation is in both (high and low) load cases present. The width of the wear track of the high-loaded situation is about 3 times bigger than the low-loaded situation. However, the total wear is closer to each other and for the rotating disc even the same value for both load cases. This means the plasticity effects are well covered by subtracting the pileup from the wear track as is discussed in subsection 5.3.

### 7.5.3 Pinion material shape

Due to the shape of the pinion materials (rounded disc in 2 directions), wear leads to an increasing contact area over time between the stationary and rotating disc. Wear on the surface creates a new plane that is closer to the centre of the disc. The length and width of each slice and thus the area of the plane will increase and thus of the contact area. A visual picture is shown in Figure 7.5. This leads to a pressure loss. This is an additional influence on the pressure next to the hardness that already

influences the maximum reachable pressure as is explained in subsection 7.1. 3GPa can be reached with the smallest radius of the ellipse being  $100\ \mu\text{m}$  and 1.5 GPa with  $50\ \mu\text{m}$ . In Figure 6.9, it can be seen that this value is increased as the smallest radius of the ellipse on the stationary discs is bigger than these required values for both loads. The non-constant pressure over time makes the results less applicable to a real situation as the pressure will be constant in a real situation. With a flat contacting surface, the pressure would have been constant during the experiments

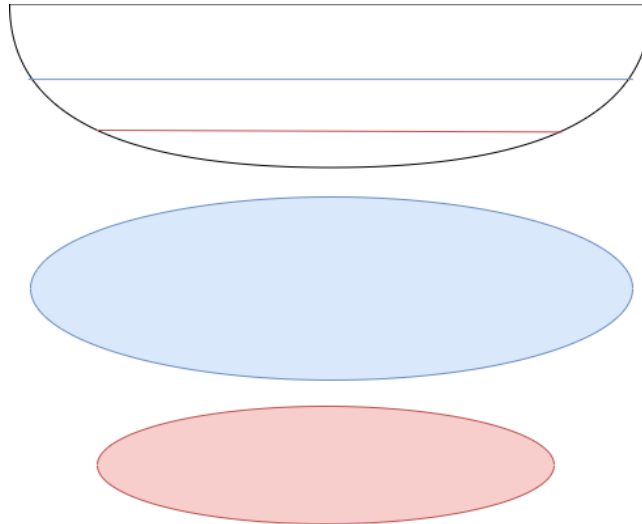


Figure 7.5: Increase in ellipse area with wear crosssectional lines. Blue has a higher area than red due to wear.

#### 7.5.4 Different shape on the uncoated disc than other pinion discs

The different shape of the uncoated disc is removed to a level within the roughness regime. However, this still influences how much wear is measured, as the exact shape is not possible to trace. It is less accurate than the laser-cladded discs. Besides this different shape must have had an influence on the amount of wear on both materials. The contact is not perfectly elliptical anymore as can be seen in Figure 5.15. How much difference is difficult to determine.

#### 7.5.5 Seawater standards

For the reproducibility of experiments, standards for the preparation of seawater are present such as ASTM D1141-98 [84]. These, however, are difficult and costly to prepare or buy. Besides, in real seawater, local differences can be present so a real situation can differ from this standard. For those reasons, it was chosen to use real Mediterranean sea salt and mix it with pure water. For both sea salt and pure water, the composition is known and thus reproducibility can be achieved by using the same water and salt.

### 7.6 Limitations of the research

In this section, the limitations of this research are discussed.

#### 7.6.1 No slide-to-roll ratio

The slide-to-roll ratio is not taken into account in this research. This means rolling contact fatigue is not measured, while in a real rack-pinion system, this is present. For that reason, a real system can

have different wear rates than this research [45]. Besides, the coefficient of friction will be lower, as rolling in combination with sliding has lower friction than pure sliding [3].

### 7.6.2 1-directional wear

Only 1 directional wear is measured in this research. In a real rack-pinion system, a motion can be in two directions. Small repetitive movements can create cyclic stresses at the surface. These can be present when controlling the movement, for example for the motion-compensated pile gripper that reacts to waves. The cyclic stresses create crack growth and in the end surface fatigue. This wear behaviour is not examined in this research.

### 7.6.3 Sliding distance

The real situation has a bigger sliding distance than is used in this research. This can be seen in the total sliding distance for 1 gear in Table 10. The lowest sliding distance is in a Jacking system that has 10507 meters of sliding distance per tooth flank, which is much higher than the experimented 60 m. The experiments are executed by measuring only one spot, so a false specific wear rate is observed when inter or extrapolating the observed values. The wear is in the stable region, so it behaves linearly at the measured sliding distance. This means the wear rate will be overestimated when the wear rates are applied to a real system service life.

Based on the results, the influence of different parameters is discussed and found. The research cannot be used to determine the service life of the different materials exactly. The research can only be used with certainty to compare the wear and coefficient of friction of the different materials in different tribological systems during pure sliding.

## 7.7 Future research

In this section possible future research is discussed.

### 7.7.1 Hypotheses of formation of oxides

In future research, the hypotheses on the formation of oxides that help in wear can be researched for the experimented tribological systems. At the point of finding this hypothesis, the samples are already corroded by general corrosion. To be able to experiment with this, a freshly worn surface with (sea) water should be analysed. This can be measured in several ways.

### 7.7.2 Match hardness of steel and stellite

To be able to exclude all hardness effects, it is required to have the same hardness on an uncoated and coated disc. This way more information can be found on the effect of a different composition on wear and friction. In future research, this effect can be experimented on by measuring the wear rate and friction.

### 7.7.3 Hardness increase of rotating disc

The original experiments were planned to research the effects of the hardness of the rack material on the wear of the uncoated and coated pinion. As previously discussed it was not possible to conclude anything from this due to too little difference in hardness. In future research, this effect can be analysed by measuring the wear rate and friction.

#### 7.7.4 Slide-to-roll ratio included in experiments

To experiment on wear and friction values of a real rack and pinion system a Slide-to-roll ratio should be applied in future research. This way, rolling contact fatigue will be present as an additional wear type. A different wear rate and friction are expected due to the added wear mechanism and the fact that rolling is known to have lower friction than pure sliding.

#### 7.7.5 Calculate if the wear reduction is enough

Based on Finite Element simulations of resulting stresses, the maximum tolerated wear can be calculated. This way can be decided if the reduction of the wear rate is permissible. If this reduction is enough with the current specific wear rate that overestimates the real value in a long-term situation, the reduction of wear with a coating is enough to apply it on a real case.

#### 7.7.6 Additives to the water

To improve efficiency and lifetime by reducing the coefficient of friction and wear, additives can be added to the water. This has to be experimented on to see the added value. Besides, to stay with the problem statement of this research, these additives should be biodegradable products.

## 8 Conclusion

This research investigated the feasibility of laser-cladded cobalt-based superalloys as a replacement for greased open gear systems. The main research question of this thesis was: *"To what extent are greaseless open gears feasible within the high-loaded systems in offshore applications?"*

The system properties of the current tribological systems selected for this research are analysed. Using the Dowson-Higginson equation for the minimum film thickness based on the base oil in the grease, the lubrication regimes are calculated. The current systems are mainly in boundary lubrication, especially in summer conditions. The other parameters found were used to construct experimental parameters that are used in the sliding wear experiments.

Disc-on-disc pure sliding wear experiments are performed to study the wear behaviour that is supported by friction data. A specific wear rate is found and the surface morphology is used to determine the wear mechanisms present.

The biggest difference in specific wear rates is found between different types of lubrication. Unlubricated wear has the highest specific wear rate with severe adhesive wear present. Seawater and pure water have similar specific wear rates. These show mild abrasive wear in combination with corrosive wear. Grease lubrication results in wear that is in the roughness regime that is too low to measure. Boundary lubrication is found to be present throughout the whole sliding distance as the friction coefficient is stable and very low.

A higher load leads to a lower specific wear rate but still, a similar wear type is present. In this case, abrasive wear with corrosive wear as seawater lubrication is used for this relation. For an increased load higher total wear is present, however, plastic deformation influences the specific wear rate. The increase in total wear is less than the increase in load. The contact area increases and thus pressure is reduced.

A higher velocity leads to less specific wear. The formation of a strong oxide layer is the best explanation based on the literature. This is continuously forming and reduces the abrasive wear. This is a hypothesis as the effect was not possible to measure.

With the same composition hardness is a factor. Within stellites an increasing hardness leads to less wear. Stellite 190 performs the best of all coatings, regarding wear. Generally, uncoated steel performs worse than at least one stellite while being harder. In (sea) water uncoated steel performs worse than all stellite coatings. The influence of hardness of rack material was not comparable, as the difference between both rack materials was very minor.

The main question can be answered using the subquestions and the limitations of the research. The proposed laser-cladded cobalt-based superalloy coatings do reduce wear compared to the uncoated material. Stellite 190 is found to be the best wear-reducing. Unlubricated wear is undesirable as severe adhesive wear is present. Sea(water) lubrication shows better performance. However, the uncoated pinion with grease lubrication which is the current situation in the observed applications performs better. It is still to be determined if the wear reduction by the coatings is enough to be feasible as a replacement for grease.



---

## References

- [1] Van Meeuwen Lubrication BV , "LUBCON GRIZZLY GREASE BIO 1-1000, NLGI 0-1," Technical Specifications, "Accessed on 16-8-2024". [Online]. Available: [www.vanmeeuwen.com](http://www.vanmeeuwen.com)
- [2] ExxonMobil, "Understanding oil bleed and grease separation," 2017.
- [3] A. van Beek, *Advanced Engineering Design: Lifetime performance and reliability*. TU Delft, 2019.
- [4] C. Wang, F. Tian, S. Zhao, G. Shang, Y. Ma, and D. Chen, "Design of monitoring ptz with high scalability," *Frontiers of Mechatronical Engineering*, vol. 2, p. 13, 05 2020.
- [5] VesselFinder, "Jan de nul group's newest jack up vessel 'voltaire' will be equipped with huisman leg encircling crane - vesselfinder," "Accessed on 30-8-2024". [Online]. Available: <https://www.vesselfinder.com/news/15225-Jan-De-Nul-Groups-newest-jack-up-vessel-Voltaire-will-be-equipped-with-Huisman-Leg-Encircling-Crane>
- [6] Kennametal Inc, "The stellite family of alloys, cobalt-based alloys." [Online]. Available: <https://www.stellite.com/us/en/alloys/stellite.html>
- [7] Kennametal Inc., "Triballoy t-400/t400-c alloys," Technical Specifications, 2021. [Online]. Available: <https://catalogs.kennametal.com/infrastructure/Triballoy-T-400-T-400C-Alloys/1/#>
- [8] M.B. de Rooij, "Failure Mechanisms Life Prediction lecture slides: Lecture 6 -Wear and lubrication- de Rooij," University of Twente, Enschede, The Netherlands, 2023.
- [9] M. Yaghoubi and H. Tavakoli, *Hertzian Contact Stress*. Cham: Springer International Publishing, 2022, pp. 5–8.
- [10] M. B. Dobrica and M. Fillon, *Mixed Lubrication*. Boston, MA: Springer US, 2013, pp. 2284–2291.
- [11] D. Dowson, "Elastohydrodynamic lubrication," *The fundamentals of roller and gear lubrication*, 1966.
- [12] A. A. Lubrecht, C. H. Venner, and F. Colin, "Film thickness calculation in elasto-hydrodynamic lubricated line and elliptical contacts: The dowson, higginson, hamrock contribution," *Proceedings of the Institution of Mechanical Engineers, Part J: Journal of Engineering Tribology*, vol. 223, pp. 511–515, 5 2009.
- [13] H. Cen and P. M. Lugt, "Film thickness in a grease lubricated ball bearing," *Tribology International*, vol. 134, pp. 26–35, 2019.
- [14] International Organization for Standardization, "Rolling bearings — explanatory notes on iso 281 — part 2: Modified rating life calculation, based on a systems approach to fatigue stresses," ISO, Technical Report ISO/TR 1281-2, 2008.
- [15] B. Hamrock, S. Schmid, and B. Jacobson, *Fundamentals of Fluid Film Lubrication*. CRC Press, 2004.
- [16] T. Tinga, "Failure mechanisms," *Springer Series in Reliability Engineering*, vol. 69, pp. 85–157, 12 2013.
- [17] E. Rabinowicz, "The effect of size on the looseness of wear fragments," *Wear*, vol. 2, no. 1, pp. 4–8, 1958.

- 
- [18] A. Tsujimoto, W. W. Barkmeier, N. G. Fischer, K. Nojiri, Y. Nagura, T. Takamizawa, M. A. Latta, and M. Miazaki, "Wear of resin composites: Current insights into underlying mechanisms, evaluation methods and influential factors," pp. 76–87, 5 2018.
- [19] Z. Zhu, C. Ouyang, Y. Qiao, and X. Zhou, "Wear characteristic of stellite 6 alloy hardfacing layer by plasma arc surfacing processes," *Scanning*, vol. 2017, 2017.
- [20] I. Radu and D. Y. Li, "Investigation of the role of oxide scale on stellite 21 modified with yttrium in resisting wear at elevated temperatures," in *Wear*, vol. 259, 7 2005, pp. 453–458.
- [21] A. Motallebzadeh, E. Atar, and H. Cimenoglu, "Sliding wear characteristics of molybdenum containing stellite 12 coating at elevated temperatures," *Tribology International*, vol. 91, pp. 40–47, 7 2015.
- [22] C. Chen and W. Meiping, "Investigation of the friction and corrosion behavior of laser-clad cobalt-based coatings in sea water," *Metal Science and Heat Treatment*, vol. 63, pp. 444–448, 11 2021.
- [23] O. Barrau, C. Boher, C. Vergne, F. Rezai-Aria, and R. Gras, "Investigations of friction and wear mechanisms of hot forging tool steels," 2002.
- [24] G. Stachowiak and A. Batchelor, *Engineering Tribology*, 4th ed. Butterworth-Heinemann, 2013.
- [25] J. Wang, B. Han, C. Wang, A. Neville, and A. Morina, "Study on the effect of graphene/fe<sub>3</sub>o<sub>4</sub> film on friction and wear performance under water lubrication," *Diamond and Related Materials*, vol. 130, 12 2022.
- [26] J. Archard, "Contact and rubbing of flat surfaces," *Journal of applied physics*, vol. 24, no. 8, pp. 981–988, 1953.
- [27] J. Hu, H. Song, S. Sandfeld, X. Liu, and Y. Wei, "Breakdown of archard law due to transition of wear mechanism from plasticity to fracture," *Tribology International*, vol. 173, 9 2022.
- [28] D. Landgeer and A.W.J. de Gee, "Tribologie – deel A: Inleiding dynamische contactverschijnselen," 1994, lecture notes, University of Twente, Enschede, The Netherlands (in Dutch).
- [29] P. J. Blau, "How common is the steady-state? the implications of wear transitions for materials selection and design," *Wear*, vol. 332, pp. 1120–1128, 2015.
- [30] K. Kato and K. Adachi, *Wear mechanisms*. CRC Press, Jan. 2000, pp. 273–300.
- [31] R. Mott and J. Tang, *Machine Elements in Mechanical Design (4th ed. in SI Units)*. Pearson Prentice Hall, 2006.
- [32] R. Errichello, *Gear Sliding*. Boston, MA: Springer US, 2013, pp. 1520–1523.
- [33] G. Meneghetti, A. Terrin, and S. Giacometti, "A twin disc test rig for contact fatigue characterization of gear materials," *Procedia Structural Integrity*, vol. 2, pp. 3185–3193, 12 2016.
- [34] D. Walton and A. J. Goodwin, "The wear of unlubricated metallic spur gears," pp. 103–113, 1998.
- [35] S. Kalpakjian, S. Schmid, and V. Sekar, *Manufacturing Engineering and Technology*, 10 2013.
- [36] Höganäs, "Atmospheric plasma spraying (aps)," "Accessed on 16-9-2024". [Online]. Available: <https://www.hoganas.com/en/powder-technologies/surface-coating/atmospheric-plasma-spraying/>
-

- 
- [37] —, “Plasma transferred arc (pta),” “Accessed on 16-9-2024”. [Online]. Available: <https://www.hoganas.com/en/powder-technologies/surface-coating/plasma-transferred-arc/>
- [38] —, “Laser cladding,” “Accessed on 16-9-2024”. [Online]. Available: <https://www.hoganas.com/en/powder-technologies/surface-coating/laser-cladding/>
- [39] M. Alam, R. J. Urbanic, S. Saqib, and A. Edrisy, “Effect of process parameters on the microstructural evolutions of laser clad 420 martensitic stainless steel,” 08 2015.
- [40] A. V. Shafranov, E. A. Morozov, K. R. Muratov, A. A. Drozdov, and A. N. Yurchenko, “Adhesive strength of cobalt-alloy coatings applied by laser surfacing on structural-steel substrates,” *Russian Engineering Research*, vol. 40, pp. 882–884, 10 2020.
- [41] J. Wen, H. Che, R. Cao, H. Dong, Y. Ye, H. Zhang, J. Brechtel, Y. Gao, and P. K. Liaw, “Evolution of the mechanical properties of a cobalt-based alloy under thermal shocks,” *Materials Design*, vol. 188, p. 108425, 2020.
- [42] Kennametal Inc., “Stellite 21 alloy,” Technical Specifications, 2020. [Online]. Available: <https://catalogs.kennametal.com/infrastructure/Stellite-21-Alloy/1/#>
- [43] J. W. Seo, J. im, S. J. Kwon, and H. K. Jun, “Effects of laser cladding for repairing and improving wear of rails,” *International Journal of Precision Engineering and Manufacturing*, vol. 20, pp. 1207–1217, 7 2019.
- [44] Kennametal Inc., “Stellite 6 alloy,” Technical Specifications, 2021. [Online]. Available: <https://catalogs.kennametal.com/infrastructure/Stellite-6-Alloy/1/#>
- [45] S. R. Lewis, R. Lewis, and D. I. Fletcher, “Assessment of laser cladding as an option for repairing/enhancing rails,” *Wear*, vol. 330-331, pp. 581–591, 5 2015.
- [46] Kennametal Inc., “Stellite 190 alloy,” Technical Specifications, 2020. [Online]. Available: <https://catalogs.kennametal.com/infrastructure/Stellite-190-Alloy/1/#>
- [47] M. X. Yao, J. B. Wu, and Y. Xie, “Wear, corrosion and cracking resistance of some w- or mo-containing stellite hardfacing alloys,” *Materials Science and Engineering: A*, vol. 407, pp. 234–244, 10 2005.
- [48] J. Tuominen, P. Vuoristo, and T. Mäntylä, “Microstructure and dry sliding wear properties of laser clad triballoy coatings,” in *PICALO 2004 - 1st Pacific International Conference on Applications of Laser and Optics, Conference Proceedings*, 2004, pp. 13–17.
- [49] Castrol, “Molub-Alloy 936 SF Heavy Open Gear Compounds (Solvent Free),” Technical Specifications, “Accessed on 16-8-2024”. [Online]. Available: [www.castrol.com/industrial](http://www.castrol.com/industrial)
- [50] Bruker Nano, Inc, “Bruker umt tribolab multi-specimen test system hardware installation manual,” Technical Specifications and accessories, 2015.
- [51] Merck millipore Ltd., “Elix® essential 3 water purification system,” Technical Specifications and accessories.
- [52] T. Sandle, “12 - depyrogenation and endotoxin,” in *Sterility, Sterilisation and Sterility Assurance for Pharmaceuticals*, ser. Woodhead Publishing Series in Biomedicine, T. Sandle, Ed. Woodhead Publishing, 2013, pp. 171–188.
- [53] VehGro B.V., “Mediterranean sea salt (fine, 0.2-1.0 mm).” [Online]. Available: [https://www.naturaplaza.nl/pdf\\_files/Specsheets/30136\\_Mediterranean\\_Sea\\_Salt\\_Fine\\_0.2-1.0\\_mm.pdf](https://www.naturaplaza.nl/pdf_files/Specsheets/30136_Mediterranean_Sea_Salt_Fine_0.2-1.0_mm.pdf)
-

- 
- [54] ASTM steel, "BS EN 42CrMo4 | 1.7225 Alloy Engineering Steel," Technical Specifications, "Accessed on 16-8-2024". [Online]. Available: <https://www.astmsteel.com/product/42crmo4-alloy-steel/>
- [55] Y. Cao, R. Hu, W. Shi, Z. Wang, M. Qiu, X. Zhang, and B. Li, "Experimental study on laser peen texturing and tribological properties of e690 high-strength steel," *Optics Laser Technology*, vol. 157, p. 108784, 2023.
- [56] ASTM steel, "1.6587 Steel: 18CrNiMo7-6 Case hardening Steels to EN 10084," Technical Specifications, "Accessed on 16-8-2024". [Online]. Available: <https://www.astmsteel.com/product/1-6587-steel/>
- [57] ZwickRoell, "Durascan micro and low-load hardness tester," Technical Specifications and accessories, 2021.
- [58] Mettler-Toledo GmbH, Laboratory Weighing Technologies, "Technical specifications and accessories mettler toledo at/mt/umt balances," Technical Specifications and accessories, 2000.
- [59] Sensofar, "S neox3d optical profiler," Technical Specifications and accessories, Copyright 2024.
- [60] Keyence, "Digital microscope vhx-7000 series," Technical Specifications and accessories, 2022.
- [61] M. Masen, *POLYFIT function*, 2001, [matlab script].
- [62] E. Tolouei, V. Hurel, A. Loucif, J.-B. Morin, and M. Jahazi, "Influence of the as quenched state and tempering temperature on the final microstructure and hardness of a high strength medium carbon steel," *Materials Chemistry and Physics*, vol. 325, p. 129765, 2024.
- [63] K. Zakowski, M. Narozny, M. Szocinski, and K. Darowicki, "Influence of water salinity on corrosion risk - the case of the southern baltic sea coast," *Environmental Monitoring and Assessment*, vol. 186, pp. 4871–4879, 2014.
- [64] L. Nedeloni, Z. I. Korca, D. T. Pascal, N. Kazamer, and M. D. Nedeloni, "Comparative study on dry sliding wear resistance of carbon steel, alloyed steel and cast iron," in *IOP Conference Series: Materials Science and Engineering*, vol. 416. Institute of Physics Publishing, 10 2018.
- [65] S. I. Hango, L. A. Cornish, L. H. Chown, J. W. van der Merwe, and F. P. Kavishe, "Sliding wear resistance of the cobalt-based coatings, ultimetm and stellite 6 with ruthenium additions," *Engineering Failure Analysis*, vol. 155, p. 107717, 2024.
- [66] K. Dohda, M. Yamamoto, C. Hu, L. Dubar, and K. Ehmann, "Galling phenomena in metal forming," *Friction*, vol. 9, pp. 1–21, 11 2020.
- [67] G. Wang, H. Zhao, Y. Zhang, J. Wang, G. Zhao, and L. Ma, "Friction and wear behavior of nm500 wear-resistant steel in different environmental media," *Crystals*, vol. 13, 5 2023.
- [68] P. Wood, H. Evans, and C. Ponton, "Investigation into the wear behaviour of stellite 6 during rotation as an unlubricated bearing at 600 °c," *Tribology International*, vol. 44, no. 12, pp. 1589–1597, 2011.
- [69] A. Gholipour, M. Shamanian, and F. Ashrafizadeh, "Microstructure and wear behavior of stellite 6 cladding on 17-4 ph stainless steel," *Journal of Alloys and Compounds*, vol. 509, no. 14, pp. 4905–4909, 2011, cited By 139.
- [70] W. Da Silva, R. Souza, J. Mello, and H. Goldenstein, "Room temperature mechanical properties and tribology of nicralc and stellite casting alloys," *Wear*, vol. 271, no. 9-10, pp. 1819–1827, 2011.

- 
- [71] J. Krell, A. Röttger, and W. Theisen, "Comprehensive investigation of the microstructure-property relationship of differently manufactured co-cr-c alloys at room and elevated temperature," *Wear*, vol. 444-445, 3 2020.
- [72] M. van Otterloo, de Hosson, S. Materialia, J. de Mol van Otterloo, and J. D. Hosson, "Microstructure and abrasive wear of cobalt-based laser coatings," *Scripta Math*, vol. 36, pp. 239–245, 1997.
- [73] L. Xu and N. F. Kennon, "A study of the abrasive wear of carbon steels," pp. 101–112, 1991.
- [74] G. Deng, A. K. Tieu, X. Lan, L. Su, L. Wang, Q. Zhu, and H. Zhu, "Effects of normal load and velocity on the dry sliding tribological behaviour of cocrfenimo0.2 high entropy alloy," *Tribology International*, vol. 144, 4 2020.
- [75] Y. Tang, P. Ji, B. Li, G. Zhang, W. Ma, F. Wang, X. Zhang, M. Ma, and R. Liu, "Effect of loading on microstructure and friction and wear behavior of an austenite lightweight steel," *Tribology International*, vol. 177, 1 2023.
- [76] H. A. Ameen, K. S. Hassan, and E. M. M. Mubarak, "American journal of scientific and industrial research effect of loads, sliding speeds and times on the wear rate for different materials," 2011.
- [77] N. Saka, A. M. Eleiche, and N. P. Suh, "Wear of metals at high sliding speeds," pp. 109–125, 1977.
- [78] J. Yao, Y. Ding, R. Liu, Q. Zhang, and L. Wang, "Wear and corrosion performance of laser-clad low-carbon high-molybdenum stellite alloys," *Optics Laser Technology*, vol. 107, pp. 32–45, 2018.
- [79] A. Dréano, S. Fouvry, and G. Guillonnet, "A tribo-oxidation abrasive wear model to quantify the wear rate of a cobalt-based alloy subjected to fretting in low-to-medium temperature conditions," *Tribology International*, vol. 125, pp. 128–140, 9 2018.
- [80] J. L. Sullivan, T. F. J. Quinn, and D. M. Rowson, "Developments in the oxidational theory of mild wear," 1980.
- [81] X. F. Qin, D. L. Sun, and L. Y. Xie, "Analysis of critical stress for subsurface rolling contact fatigue damage assessment under roll/slide contact," pp. 61–67, 2 2014.
- [82] G. M. Hamilton and L. Goodman, "The stress field created by a circular sliding contact," 1966.
- [83] M. Gargourimotlagh and M. de Rooij, "The effect of highly elongated micro-contacts on rolling contact stress field," *Tribology International*, vol. 196, 8 2024.
- [84] American Society for Testing and Materials (ASTM), "Standard practice for preparation of substitute ocean water," ASTM International, West Conshohocken, PA, USA, Standard D1141-98 (Reapproved 2021), 2021.
- [85] W. Ya and B. Pathiraj, "Residual stresses in stellite 6 layers cladded on aisi 420 steel plates with a nd:yag laser," *Journal of laser applications*, vol. 30, no. 3, Jul. 2018.
- [86] W. Ya, B. Pathiraj, D. T. Matthews, M. Bright, and S. Melzer, "Cladding of triballoy t400 on steel substrates using a high power nd:yag laser," *Surface and Coatings Technology*, vol. 350, pp. 323–333, 9 2018.



## A Cracking and chipping on production

While turning on a lathe with a diamond tool, Tribaloy T-400 showed chipping as can be seen in Figure A.1. The material consists of a very hard phase (carbides) within a softer solution [7]. These formed carbides are hard and brittle [85]. This material is very hard to apply since the material is required to be preheated to avoid cracking [86]. Nonlinear shrinkage and different cooling rates from the steel it is applied to can cause tensile residual stress [85]. When this exceeds the yield strength of the cladded layer (T-400 has a lower yield strength than high-grade steel [7], due to the brittleness of carbides), this layer will start cracking as a failure.



5 mm

Figure A.1: Chipping of Tribaloy T-400 during the turning process